JLAB-THY-98-24

INTERACTION, CURRENTS AND THE ELECTROMAGNETIC STRUCTURE OF LIGHT NUCLEI

L. E. Marcucci
Department of Physics, Old Dominion University, Norfolk, Virginia 23529

R. Schiavilla
Jefferson Lab, Newport News, Virginia 23606
and
Department of Physics, Old Dominion University, Norfolk, Virginia 23529

We discuss the traditional model of the nucleus as a system of nucleons interacting via effective interactions and currents, and present results obtained within this framework for the electromagnetic structure of the ground- and low-lying-states of A=3–6 nuclei.

1 Introduction

In these lectures we discuss the traditional picture of the nucleus as a system of nucleons interacting via effective interactions and currents. Light nuclei provide the ideal ground for testing this dynamical framework, since they are amenable to numerically "exact" and/or accurate calculations.

The lectures are organized as follow. We first discuss the nature of the nuclear Hamiltonian. In particular, we review models for the two- and three-nucleon interactions, as well as current approaches to the treatment of the relativistic few-nucleon problem.

The second part of the lectures is devoted to a discussion of the methods used to solve the Schrödinger equation. This discussion is here slanted towards quantum Monte Carlo (QMC) methods. Apart from our personal bias, the reason is that QMC methods, both in the variational Monte Carlo (VMC) and Green's function Monte Carlo (GFMC) versions, have proven to be well suited to deal with systems with A=3–8. This, of course, does not do justice to the other techniques, such as Faddeev-Yakubowsky, correlated hyperspherical harmonics (CHH), stochastic variational methods, which have been developed in recent years to deal with few-nucleon systems. However, studies based on these techniques have been limited so far to three- and four-nucleon systems, and are therefore somewhat more specialized and less flexible than QMC.

Finally, in the third part of the lectures we discuss succintly the nuclear electromagnetic charge and current operators, and the relation between these

and the measured elastic and inelastic form factors of few-nucleon systems.

A more complete discussion of these topics can be found in a review paper by Carlson and one of the authors here (R.S.) [1].

2 Nuclear Hamiltonian

We consider the simplest picture of a nucleus, a system of interacting neutrons and protons. In a non-relativistic framework, the Hamiltonian is:

$$H = \sum_i \frac{\mathbf{p}_i^2}{2m} + \sum_{i<j} v_{ij} + \sum_{i<j<k} V_{ijk} + \cdots, \tag{1}$$

where the nucleons interact via two-, three-, and possibly many-body interactions. Studies of the nuclear interaction, both experimental and theoretical, have a long history, beginning essentially with the discovery of the neutron by Chadwick in 1932, and proceeding through the justification of this simple picture of nuclei within QCD by Weinberg [2]. A nice review of much of this history, along with a detailed description of current nucleon-nucleon (NN) interaction models, is given by Machleidt [3]. Here we merely explain some of the dominant features of the NN interaction and their importance in the structure and dynamics of light nuclei.

2.1 Two-nucleon interactions

The NN interaction has an extraordinarily rich structure, as has been recognized for quite a long time. It is described in terms of the nucleon's spin ($\frac{1}{2}\boldsymbol{\sigma}$) and isospin ($\frac{1}{2}\boldsymbol{\tau}$), where both $\boldsymbol{\sigma}$ and $\boldsymbol{\tau}$ are Pauli matrices. The former variable represents the intrinsic angular momentum (spin) of the nucleon, while the latter is a convenient representation for its two charge states–the proton and neutron. The generalized Pauli principle in this framework requires that two-nucleon states be antisymmetric with respect to the simultaneous exchange of the nucleons' space, spin, and isospin coordinates. The predominant isospin-conserving part of the NN interaction is written as linear combinations of components proportional to the two isoscalars, 1 and $\boldsymbol{\tau}_i \cdot \boldsymbol{\tau}_j$.

The long-range component of the NN interaction is due to one-pion-exchange (OPE). If isospin-breaking terms are ignored, it is given, at long distances, by:

$$v_{ij}^{OPE} = \frac{f_{\pi NN}^2}{4\pi} \frac{m_\pi}{3} \left[Y_\pi(r_{ij}) \boldsymbol{\sigma}_i \cdot \boldsymbol{\sigma}_j + T_\pi(r_{ij}) S_{ij} \right] \boldsymbol{\tau}_i \cdot \boldsymbol{\tau}_j, \tag{2}$$

$$Y_\pi(r_{ij}) = \frac{\mathrm{e}^{-\mu r_{ij}}}{\mu r_{ij}} \tag{3}$$

$$T_\pi(r_{ij}) = \left[1 + \frac{3}{\mu r_{ij}} + \frac{3}{(\mu r_{ij})^2} \right] \frac{\mathrm{e}^{-\mu r_{ij}}}{\mu r_{ij}}, \tag{4}$$

where m_π is the mass of the exchanged pion, and

$$S_{ij} \equiv 3\, \boldsymbol{\sigma}_i \cdot \hat{\mathbf{r}}_{ij} \boldsymbol{\sigma}_j \cdot \hat{\mathbf{r}}_{ij} - \boldsymbol{\sigma}_i \cdot \boldsymbol{\sigma}_j \tag{5}$$

is the tensor operator. At distances comparable to the inverse pion mass ($1/\mu \approx 1.4$ fm), OPE leads to a large tensor component in the NN interaction. In nuclear systems, then, the spatial and spin degrees of freedom are strongly correlated, and hence nuclear few- and many-body problems can be quite different from systems where the dominant interaction is independent of the particles internal quantum numbers (spin and isospin), such as the Coulomb interaction in atomic and molecular problems or Van der Waals forces in systems like bulk Helium.

To further illustrate this point, we reproduce in Fig. 1 the plots of the deuteron's nucleon densities for two different orientations of the pair's spin, $S_z = \pm 1$ and $S_z = 0$, respectively [4]. Surfaces of constant nucleon density for the two different spin orientations are displaied, and, as is apparent in the figure, the density is strongly correlated with the nuclear spin. Similar structures in the two-body distributions seem to occur in all light nuclei [4]. While this figure was constructed using a particular model of the NN interaction, the Argonne v_{18} [5], any NN interaction including short-range repulsive and long-range tensor components would produce a nearly indistinguishable plot.

At moderate and short distances, the NN interaction is much more complicated. However, the large body of pp and pn scattering data accumulated over the past half century provides, by now, very strong constraints, and indeed has been crucial in advancing our knowledge of the NN interaction.

In the short- and intermediate-distance region, the interaction models can be quite different, ranging from one-boson-exchange (OBE) models to models with explicit two-meson-exchanges to purely phenomenological parametrizations. Examples include the Paris [6], Bonn [7], Nijmegen [8], and Argonne v_{14} [9] interaction models. The Nijmegen group employed Regge pole theory to obtain an NN interaction model which includes numerous OBE terms with exponential form factors at the vertices, plus repulsive central Gaussian potentials arising from the Pomeron and tensor trajectories. This Nijmegen interaction is mildly non-local in the sense that it contains at most two powers of the

nucleon pair's relative momentum. The resulting interaction can be written:

$$v_{ij}(r) = \sum_p v^p(r)\ O^p_{ij} \qquad (6)$$

where the operators O^p_{ij} are products of

$$O^p_{ij} = [1, \sigma_i \cdot \sigma_j\ , S_{ij}\ , (\mathbf{L}\cdot\mathbf{S})_{ij}\ , \mathbf{p}^2_{ij}\ , \mathbf{p}^2_{ij}\sigma_i \cdot \sigma_j\ , (\mathbf{L}\cdot\mathbf{S})^2_{ij}] \otimes [1,\ \tau_i \cdot \tau_j], \quad (7)$$

$\mathbf{p}_{ij} = (\mathbf{p}_i - \mathbf{p}_j)/2$ is the relative momentum of the pair, and $\mathbf{L}$ is the relative orbital angular momentum. The radial forms $v^p(r)$ are obtained from meson exchanges with phenomenological form factors. The coupling constants and form factor cutoffs are then adjusted to fit the deuteron properties and NN scattering data.

The Bonn group[7] used "old-fashioned" time-ordered perturbation theory, and included a number of OBE terms, plus two-meson-exchanges (2π, $\pi\rho$, and $\pi\omega$), correlated two-pion-exchange (TPE) in the form of the exchange of an effective scalar meson (the σ-meson), effective three-pion-exchange, and intermediate Δ-isobars. Several forms of the Bonn interaction were presented; of these, the "full" Bonn interaction is energy-dependent and consequently difficult to use in many-body calculations. The Bonn B interaction is often used in realistic calculations, it is an energy-independent model constructed in momentum-space; in coordinate space it contains non-localities with the range of the nucleon's Compton wavelength (≈ 0.2 fm).

The Argonne v_{14} (AV14) interaction[9] is of a more phenomenological form. At short and intermediate distances, its radial dependence is parametrized as a sum of functions proportional to T^2_π, defined in Eq. (4), and consequently of two-pion-exchange range, plus short-range Woods-Saxon functions. The magnitude of these terms, as well as the parameters of the Woods-Saxon radial shapes, are adjusted to fit the data. As the Nijmegen interaction, the AV14 is a mildly non-local interaction containing at most two powers of the relative momentum. However, the AV14 interaction uses the operators:

$$O^p_{ij} = [1, \sigma_i \cdot \sigma_j\ , S_{ij}\ , (\mathbf{L}\cdot\mathbf{S})_{ij}\ , \mathbf{L}^2_{ij}\ , \mathbf{L}^2_{ij}\sigma_i \cdot \sigma_j\ , (\mathbf{L}\cdot\mathbf{S})^2_{ij}] \otimes [1,\ \tau_i \cdot \tau_j]\ . \quad (8)$$

The first eight of these operators (those not involving two powers of the momentum) are unique in the sense that all such operators are implicitly contained in any realistic NN interaction model. The choice of the higher-order terms involving the second power of the orbital angular momentum operator is different than in the Nijmegen model, which uses instead $\mathbf{p}^2$ operators in place of $\mathbf{L}^2$. The primary motivation for this choice is convenience in few- and many-body calculations, as the $\mathbf{L}^2$ terms do not contribute in relative S-waves.

The Paris interaction[6] is somewhat of a hybrid model. At intermediate NN separations, it includes single ω-meson exchange along with TPE contributions calculated using πN phase shifts, $\pi\pi$ interactions, and dispersion relations. In addition, it contains short range phenomenological terms. Indeed, all models should be considered phenomenological at short distances; they are either written phenomenologically from the start or, in the case of boson-exchange models, include phenomenological meson-nucleon form factors.

Even within the boson-exchange-type models, the interaction should not be taken literally as the exchange of single bosons. OBE models often incorporate an effective scalar σ-meson, which models the effects of correlated TPE, its mass and coupling constant being among the parameters that are adjusted to fit the two-nucleon data. Also, the relatively hard form factors obtained in NN interaction models can be thought of as simulating the exchange of heavier mesons with the same quantum numbers, or of simulating other physical effects outside the direct scope of the model.

While these models all produce a qualitatively similar picture of the NN interaction, with OPE at long range, an intermediate range attraction and a short range repulsion, quantitatively they can be somewhat different. There are several reasons for this, chief among them is that they have not all been fit to the same data. For example, models fit to np data do not precisely fit the experimental pp data if only electromagnetic corrections are introduced.

Fortunately, high quality phase shift analyses of the pp and np data have become available recently[10,11]. For example, the Nijmegen analysis relies upon the (known) long-distance electromagnetic and OPE interactions, and makes a simple energy-dependent parametrization of the interior ($r < 1.4$ fm) region. The data and analysis are quite accurate, yielding a χ^2 very near one per degree of freedom. The analysis is carried out for both pp and np experimental data, and the accuracy is sufficient to "reproduce the experimental charged and neutral pion masses" from the NN data[11]. The Nijmegen group has also attempted to determine the πNN coupling constant from the phase shift analysis[12], and find a slightly lower value ($f^2_{\pi NN}/4\pi = 0.075$) than that obtained previously. This particular result is in agreement with recent analysis of πN data[13], but is still a matter of some dispute[14–16]. Another high-quality phase shift analysis has been completed by the VPI group[10].

Recently, several NN interaction models have been fit to the experimental database. These include updated Nijmegen interactions (Nijm I, NijmII, and Reid93)[17], the Argonne v_{18} (AV18) interaction[5], and the CD Bonn interaction[18]. These models follow basically along the lines of their predecessors, however in order to provide a precise fit, they are adjusted separately to the np and pp database, which requires them to contain charge-symmetry-breaking

(CSB) terms of both isovector ($\tau_{i,z}+\tau_{j,z}$) and isotensor ($3\tau_{i,z}\tau_{j,z}-\tau_i\cdot\tau_j$) type. Each of these models fit the NN database extremely well, with χ^2 per degree of freedom near one. The cost of this excellent fit is a rather large number of parameters; the AV18 interaction has 40 adjustable parameters and the other modern interaction models have a similar number.

In these modern interaction models that contain isospin-breaking terms, the electromagnetic interaction must be specified along with the strong interaction in order to precisely reproduce the data, and consists of one- and two-photon Coulomb terms, Darwin-Foldy and vacuum polarization contributions, and magnetic moment interactions [19]. The full NN interactions, then, are the sum of a (dominant) isospin-conserving strong interaction, specified electromagnetic interactions, and finally additional isospin-breaking terms. The latter, for example, are introduced in the AV18 interaction as terms proportional to:

$$O_{k=15\ldots18} = T_{ij}\ ,\ \sigma_i\cdot\sigma_j T_{ij}\ ,\ S_{ij}T_{ij}\ ,\ (\tau_{i,z}+\tau_{j,z})\ \ , \tag{9}$$

where the isotensor operator is

$$T_{ij} = 3\tau_{i,z}\tau_{j,z} - \tau_i\cdot\tau_j\ \ . \tag{10}$$

OPE includes effects of charged versus neutral pion mass differences. In principle one could use different coupling constants for the different charge channels, however the Nijmegen analysis finds no necessity for this and the AV18 interaction uses $f^2_{\pi NN}/4\pi$=0.075 in all cases. This sophisticated fitting of the two-body np and pp data, as well as the nn scattering length, allows the study of isospin-breaking effects in three-, six-, and seven-nucleon systems.

The properties of the deuteron obtained with these interactions are given in Table 1. The binding energy E_d = 2.224575(9) MeV [20] has been fit by construction; the asymptotic constants A_S (the S-wave normalization) and η (the D/S state ratio) which govern the wave function at large distances are also quite accurate. The quadrupole moment Q_d and magnetic moment μ_d are under-predicted in the impulse approximation; however, the latter has significant corrections from two-body current operators and relativistic corrections, as will be discussed below.

The phase shifts for several channels are displayed in Figs. 2–5[5]. In Fig. 2 the np and pp phases are shown explicitly to demonstrate the difference between the np and pp interaction. Several recent phase shift analyses [10,11,21,22] are also shown. In the $^1S_0$ channel (S=0, T=1, L=0), the two sets are both strongly attractive near threshold, indicating the presence of a nearly bound state in that channel. The phase shifts differ by nearly 10 degrees near the

maximum, however. For somewhat higher energies, the interaction remains attractive, but the phase shift turns negative near 250 MeV in the lab frame. The results of several phase shift determinations are also shown in the figure.

The mixing parameter ϵ_1 is shown in Fig. 3, where it is again compared to several analyses. As is apparent, significant discrepancies remain among various analyses in that channel. This has been a subject of much debate, particularly with regard to comparisons of single- and multi-channel phase shift analyses. Nevertheless, the behavior of all the modern interaction models are all quite similar in this regard. The ϵ_1 phase is particularly sensitive to the strength of the NN tensor interaction.

More typical is the case of the $^3S_1$ phase presented in Fig. 4, for which all modern interaction models produce nearly identical results, in agreement with the Nijmegen analysis. Finally, the ^3P_J phase shifts are presented for the various interactions in Fig. 5.

2.2 Beyond static two-nucleon interactions

The Nijmegen and Argonne v_{18} interactions contain non-localities only at the level of two powers of the relative momentum (p^2 or L^2), and have been found to yeld nearly identical results for the triton binding energy, 7.62±0.01 MeV as compared to the experimental 8.48 MeV. A natural question, then, is what other effects are important in reproducing binding energies of light nuclei and triton in particular? Two of them are immediately apparent, relativistic corrections and three-nucleon interactions. It has long been known that these effects cannot be completely separated, they are related both theoretically and phenomenologically, phenomenologically in the sense that simple estimates of their contributions are comparable.

The simplest estimate of relativistic corrections is to consider a standard non-relativistic calculation of the α-particle. The total kinetic energy is on the order of 100 MeV, or 25 MeV per particle. Thus one would expect relativistic corrections on the order of 2% of this value, or 2 MeV. Three-body forces can be similar in size; at the longest distances the three-body force is of the well-known Fujita-Miyazawa type [23], corresponding to two-pion exchanges between three nucleons with the intermediate excitation of a Δ-isobar resonance. The presence of this relatively low-lying resonance requires a three-nucleon interaction at a similar level, roughly a few MeV in the α-particle.

A wide variety of relativistic calculations of light nuclei has been carried out. One-boson-exchange mechanisms can be naturally extended to relativistic treatments; such a scheme naturally leads to a four-dimensional representation of the NN interaction. Rupp and Tjon [24] have investigated trinucleon binding

as well as other properties within a separable approximation to the Bethe-Salpeter (BS) equation, and have found an increase in binding compared to non-relativistic approaches.

Several groups have pursued relativistic one-boson-exchange calculations within various three-dimensional reductions of the BS equation. These groups generally find a larger binding in the three-body system than is obtained in non-relativistic calculations; for example, Machleidt, Sammarruca, and Song[18] have fit the NN data within a OBE model using a Blankenbecler-Sugar (BbS) reduction. The resulting quasipotential equation can be cast into a form identical to the Lippman-Schwinger equation, thus allowing a direct comparison with standard non-relativistic results. Clearly, though, any three-dimensional reduction is not unique. Upon extending the BbS formalism to the three-nucleon system, Machleidt *et al.* find a triton binding energy of 8.19 MeV. Most of the additional binding is retained even in a non-relativistic version of the calculation, the additional binding in such a calculation (8.0 MeV) is attributed to the non-local character of the interaction obtained within the BbS formalism.

Trinucleon properties have also been investigated within the context of the Gross or spectator equation, in which one particle is placed on shell in all intermediate states. This scheme has the advantage of having the correct Dirac equation limit when one of the particles has a very large mass. The NN scattering and deuteron properties were originally investigated by Gross, Van Orden and Holinde[25]. Recently, Stadler and Gross[26] have introduced off-shell couplings in their OBE model. The triton binding energy has been found to be sensitive to them. In particular, a set of parameters which reproduces NN data reasonably well also yields the correct binding energy.

It is important to realize, though, that many of these corrections are scheme-dependent. For example, different choices of πNN couplings, when converted to two- and three-nucleon interactions, are connected by unitary transformations. These different choices are exactly equivalent at the static level; however, when going beyond the static level, arbitrary parameters associated with the unitary transformation are introduced. Different choices in the non-static NN interaction also yield different three-nucleon interactions. Since they are unitarily equivalent, physical properties must be unchanged[27,28]. The relationship between off-shell effects in the NN interaction and the choice of three-nucleon interactions has also been discussed by Polyzou and Glöckle[29].

Without resorting to the specific OBE mechanism, it is also possible to define the general properties of relativistic Hamiltonians which do not introduce antinucleon degrees of freedom. Within such a formalism the Poincaré invariance of the theory plays a pivotal role. The formal requirements of the theory

have been presented in an article by Keister and Polyzou[30]. Information on the underlying dynamics is outside the requirements of Poincaré invariance, and hence must be introduced from elsewhere. Fully relativistic calculations within the relativistic Hamiltonian formalism are not yet well-developed. Glöckle, Lee, and Coester[31] have investigated the triton in a simple model, however, and have found less binding than in comparable non-relativistic calculations.

Another way to perform relativistic calculations is within a (v/c) expansion scheme, where terms proportional to powers of the inverse of the nucleon mass are added to the Hamiltonian in order to preserve the Poincaré invariance to that order. Such a procedure is based upon the work of Foldy[32], Krajcik and Foldy[33], and Friar[34]. One class of relativistic corrections that has been considered in such a scheme is purely kinematical. By replacing the non-relativistic kinetic energy with the corresponding relativistic expression, and including a frame dependence in the two- (and three-) nucleon interactions,

$$H = \sum_i \sqrt{\mathbf{p}_i^2 + m^2} + \sum_{i<j} v_{ij}(\mathbf{r}_{ij}; \mathbf{P}_{ij}) + \sum_{i<j<k} V_{ijk}(\mathbf{r}_{ij}, \mathbf{r}_{ik}; \mathbf{P}_{ijk}) \ , \quad (11)$$

it is possible to construct a Hamiltonian with the correct transformation properties up to order $(v/c)^2$. In this equation, $\mathbf{P}_{ij}$ and $\mathbf{P}_{ijk}$ are the total momentum of the two- and three-body subsystems, respectively, while the dependence upon the relative coordinate is explicitly displayed. The Hamiltonian is non-local through the kinetic energy operator and the frame dependence, but the non-locality is rather small, on the order of the nucleon's Compton wavelength[35].

To perform such a calculation, it is necessary to first refit the NN data and two-body binding energy with the above Hamiltonian. The results of a comparison with a phase-equivalent non-relativistic model are somewhat surprising, in that these relativistic corrections to three- and four-body binding are in fact fairly small and repulsive; approximately 0.3 MeV of repulsion in the triton and almost 2 MeV in the α-particle. Similar estimates for these kinematical effects have been found by Stadler and Gross in the framework mentioned above. The small effect is primarily understood as a cancellation between the change to a "softer" kinetic energy operator and the revised NN interaction which must be more repulsive to yield the same phase shifts. The resulting nucleon momentum distributions are in fact quite similar in these relativistic and non-relativistic calculations[35].

Of course, other non-localities will appear in the NN interaction. At long distance these are introduced by relativistic corrections to OPE, and similar corrections would be expected in a OBE picture through vector and scalar

meson exchange. The v/c expansion scheme is currently being extended to treating the non-localities associated with OPE. These non-localities are required for a fully consistent treatment of the two-body charge operator and the nuclear Hamiltonian, and are naturally present in a relativistic OBE calculation. However, various technical difficulties make calculations of heavier systems more difficult within the OBE scheme; more direct comparisons of the different relativistic calculations will undoubtedly prove instructive in understanding all the various results obtained to date.

Three-nucleon interactions can also arise from the internal structure of the nucleon. Since all degrees of freedom other than the nucleons have been integrated out, the presence of virtual Δ-isobar resonances induces three-body forces. The longest-ranged term involves the intermediate excitation of a Δ-isobar, with pion exchanges involving two other nucleons. The two-pion-exchange three-nucleon interaction (2πTNI) was originally written down by Fujita and Miyazawa[23]:

$$V_{ijk}^{2\pi} = A_{2\pi}\left[\{X_{ij}\,,\, X_{ik}\}\,\{\tau_i\cdot\tau_j\,,\,\tau_i\cdot\tau_k\} + \frac{1}{4}\,[X_{ij}\,,\, X_{ik}]\,[\tau_i\cdot\tau_j\,,\,\tau_i\cdot\tau_k]\right]\,, \tag{12}$$

where

$$X_{ij} = Y_\pi(r_{ij})\sigma_i\cdot\sigma_j + T_\pi(r_{ij})S_{ij}\quad . \tag{13}$$

This interaction is attractive in light nuclei. Of course, other effects enter as well; several groups[36–38] have performed calculations with explicit Δ-isobar degrees of freedom in the nuclear wave functions. They generally find that the attraction from the long range two-pion-exchange TNI is canceled by dispersive effects at shorter distances and hence there is little net attraction.

Within a nucleons-only picture, several explicit models of the three-nucleon interaction have been proposed. One of them was put forward by the Tucson-Melbourne group[39], a three-nucleon interaction based upon a pion-nucleon scattering amplitude derived using PCAC, current algebra, and phenomenological input. This interaction contains the long-range 2πTNI, but also has additional structure at shorter distances. More recent versions[40] contain ρ-exchange as well as pion-range forces between the three-nucleons, with the π-ρ components of the interaction being repulsive in light nuclei. These models have been used in many different calculations, and the short-distance πNN cutoff can be adjusted to reproduce the triton binding energy. The cutoff

dependence of the results is significantly smaller in models which include ρ-exchange[41].

Another model has been derived by the Brazilian group[42–45], by using tree-level diagrams of effective Lagrangians which are approximately invariant under chiral and gauge transformations. After proper adjustments of the parameters, the resulting force gives similar results in the trinucleon bound-states as the Tucson-Melbourne model. Recent studies of this model are presented in Ref.[41].

A somewhat different approach has been taken by the Urbana-Argonne group[46,47]. Given the uncertainties in the three-nucleon interaction at distances shorter than pion-exchange, the interaction is taken as the sum of the 2πTNI plus a shorter-range term:

$$V_{ijk} = V_{ijk}^{2\pi} + V_{ijk}^{R}, \tag{14}$$

with

$$V_{ijk}^{R} = U_0 \sum_{ijk\ \mathrm{cycl}} T_\pi^2(r_{ij})T_\pi^2(r_{ik})\quad . \tag{15}$$

The second term is of two-pion exchange range on each of the two legs. It is meant to simulate the dispersive effects which are required when integrating out Δ-isobar degrees of freedom. These terms are repulsive, and are here taken to be independent of spin and isospin.

The constants $A_{2\pi}$ and U_0 in front of the two terms are adjusted to reproduce the triton binding energy, and to provide additional repulsion in hypernetted-chain variational calculations of nuclear matter near equilibrium density. However, the resulting value for the $A_{2\pi}$ coefficient is close to that obtained from the analysis of observed pion-nucleon scattering. Clearly the energy levels of light nuclei must be well reproduced if accurate predictions of other observables at low and intermediate energy transfers are to be obtained. Since one of the major goals is to tie together the medium- and low-energy properties of light nuclei, it is natural to make simple assumptions about the nature of the TNI in pursuit of that goal.

Undoubtedly the real situation is much more complicated: relativistic effects and a significantly more complicated three-nucleon interaction are certainly present. It will take far more than calculations of trinucleon binding energies to shed light on these questions. For example, calculations of three-nucleon scattering observables are, on occasion, at variance with the experimental data. Also, the isospin dependence of the TNI could prove crucial in studying light neutron-rich nuclei and neutron stars. Given recent improvements in experimental data and few-body techniques, though, it is quite possible that a more thorough understanding of these issues will be soon realized.

3 Quantum Monte Carlo methods

Given a model for the nuclear Hamiltonian, a first and important test is solving for the nuclear ground-states. Although the nuclear interaction models described above are simple to write down, solutions have proven to be rather difficult to obtain. For the three-nucleon system, there is a long history of numerical solutions to the Faddeev equations. The first calculation for local potential models without tensor interactions were obtained in Refs. [48,49]. By now, a variety of methods have been used for studying spectra of light nuclei: Faddeev-Yakubowsky, correlated hyperspherical harmonics (CHH), and variational and Green's function Monte Carlo methods. As mentioned in the Introduction, here we will only review the quantum Monte Carlo methods, and refer the reader to a recent review [1] for a discussion of the other methods.

Monte Carlo methods have often proven useful in the study of strongly-interacting quantum systems, and few-nucleon systems are no exception. They are primarily useful when explicit numerical schemes such as Faddeev or CHH methods cannot be carried out because the dimensions of the necessary grids grow too large. Two principle Monte Carlo schemes have been developed–variational and Green's function Monte Carlo.

Variational Monte Carlo (VMC) is an approximate variational method that uses Monte Carlo techniques to perform standard numerical quadratures. Diffusion or Green's function Monte Carlo (GFMC) methods, on the other hand, employ Monte Carlo methods to evaluate the imaginary-time path integrals relevant for a light nucleus. They typically use the VMC wave functions as a starting point, and cool them in order to measure ground-state observables. In this section we describe their application to ground-state properties; each can also be employed to gain information about nuclear dynamics.

3.1 Variational Monte Carlo

Variational Monte Carlo (VMC) employs an explicit form of a trial wave function, typically containing 20-30 variational parameters. These parameters are optimized by minimizing the expectation value of the energy; Monte Carlo methods, specifically the Metropolis *et al.* [50] algorithm, are used to evaluate the spatial integrals.

The trial wave functions used in VMC calculations typically have a simple form:

$$|\Psi_T\rangle = \left[\mathcal{S}\prod_{i<j<k} F_{ijk}\right]\left[\mathcal{S}\prod_{i<j} F_{ij}\right]|\Psi_J\rangle, \qquad (16)$$

where $\mathcal{S}$ represents the symmetrization operator, respectively, acting over the

A-particle space. In this equation for $|\Psi_T\rangle$, the Jastrow state $|\Psi_J\rangle$ carries the quantum number information and, for $A > 4$, much of the long-distance physics. Important clustering properties and binding or threshold effects are incorporated here. The Jastrow wave function $|\Psi_J\rangle$ is written as:

$$|\Psi_J\rangle = \mathcal{A}\left[\prod_{i<j\in s} f^c_{ss}(r_{ij}) \prod_{i\in s, j\in p} f^c_{sp}(r_{ij}) \prod_{i\in p, j\in p} f^c_{pp}(r_{ij})|\Phi\rangle\right], \qquad (17)$$

where $\mathcal{A}$ is the antisymmetrization operator. The central pair correlations f^c are functions of the pair distance only. However, the long-distance behavior may be different for nucleons in different shells, and hence the f^c are labeled by the single-particle orbits of the two nucleons. The determination of these Jastrow factors is described below. For these larger systems, $|\Phi\rangle$ is written as a sum over a small number of shell model configurations, and the coefficients of the various configurations being variational parameters.

For example, in recent calculations of six-body nuclei [47]:

$$|\Phi(JMTT_z)\rangle = \mathcal{A}[\Phi_a(00)\phi_p(r_{5,a})\phi_p(r_{6,a})] \times \sum_{L,S}\beta_{JLS}\left[[Y_1(\Omega_{5,a})Y_1(\Omega_{6,a})]_L[\chi_5\chi_6]_S\right]_{JM} \times [\eta_5\eta_6]_{TT_z}, \qquad (18)$$

where $|\Phi_a(00)\rangle$ is an antisymmetrized product of four-nucleon spinors coupled to J=T=0 with no spatial dependence, and the spatial dependence in the p-wave orbitals ϕ_p is taken from the solution of a single nucleon in a Woods-Saxon well. Additional clustering properties, for example the α-d breakup in A=6, as well as three-body correlations can also be incorporated in the Jastrow wave function if they are found to be important. Note that the wave function is translationally invariant in that it involves only pair separations and the separation between p-shell nucleons and s-shell clusters. The wave functions Ψ_J are constructed to be eigenstates of the total momentum **J**. Since the pair correlation operators commute with **J**, the total wave function also has good total angular momentum.

The "two-body" spin-isospin correlation operators F_{ij} in Eq. (16) carry the short and intermediate-range physics, including the tensor correlations and the isospin dependence in the short-range repulsion. They are parametrized as:

$$F_{ij} = \left[1 + \sum_{m=2,8} u_m(\mathbf{r}_{ij};\mathbf{R})O^m_{ij}\right], \qquad (19)$$

containing operators O^m_{ij} that are a subset of those employed in the interaction:

$$O^m_{ij} = [1,\ \boldsymbol{\sigma}_i\cdot\boldsymbol{\sigma}_j,\ S_{ij},\ (\mathbf{L}\cdot\mathbf{S})_{ij}] \otimes [1, \boldsymbol{\tau}_i\cdot\boldsymbol{\tau}_j]\,. \qquad (20)$$

The product $f^c(r_{ij})F_{ij}$ is required to satisfy the short-distance properties of the wave function as two nucleons are brought close together. The dependence upon the pair distance r_{ij} is obtained as a solution of Schrödinger-like equations in the various two-body channels. These correlations are obtained from equations similar to those used for the low-density limit of Fermi-hypernetted-chain variational calculations of nuclear matter [51,52]. Schematically, they are written as:

$$-(1/m)\nabla^2[f(r)\phi(\mathbf{r})]_{JST} + [v_{ij} + \lambda(r)][f(r)\phi(r)]_{JST} = 0 \ . \qquad (21)$$

This equation is solved for the various J, S, T channels and the correlations are recast into the operator form, as in Eq. (19). The functions $\phi(\mathbf{r})$ contain the appropriate spherical harmonics for the given channel. For the spin triplet channels the combination $[f(r)\phi(\mathbf{r})]_{JST}$ satisfy two coupled equations with L=J-1 and L=J+1 [53]. The variational parameters are included in the functional form of $\lambda(r)$. For s-shell nuclei the form is adjusted so that

$$[f^c_{\rm ss}(r)]^{A-1} \rightarrow \exp(-\gamma r)/r, \qquad (22)$$

where γ is related to the separation energy of the last nucleon. Spin dependence in the breakup channels can be treated by including a non-zero long-distance behavior in the spin dependent correlations $u_m(r)$. For larger systems, however, the product of the $f_{\rm sp}$ or $f_{\rm pp}$ in $|\Psi_J\rangle$ times the F_{ij} are adjusted to go to a constant. The pair correlation functions F_{ij} are defined to carry the spin-isospin dependence of only particles i and j. However, the associated amplitudes u_m are functions of the coordinates of all the nucleons; the presence of the remaining particles requires a quenching of the non-central correlations. The full structure of this quenching is described in Ref. [52].

The structure of the three-nucleon correlations F_{ijk} can, in principle, be quite complicated. The most important correlation is that due to the three-nucleon interaction V_{ijk}, and the operator form is taken from:

$$F_{ijk} = 1 - \beta V_{ijk}, \qquad (23)$$

where β is again a variational parameter. Additional three-body correlations have been investigated by Arriaga, Pandharipande and Wiringa [52].

Given the wave function, one can in principle evaluate the expectation value of any operator using Metropolis Monte Carlo techniques. VMC methods have often been employed in studies of other quantum systems, including, for example, atoms and molecules, the electron gas, and liquid and solid Helium. The state dependence of the interaction, though, requires a somewhat different treatment than is traditionally used in VMC calculations. Typically,

one uses the Metropolis method to obtain points distributed proportional to a probability density $W(\mathbf{R})$, often choosing $W(\mathbf{R}) = |\langle\Psi_T(\mathbf{R})|\Psi_T(\mathbf{R})\rangle|$, where the angled brackets indicate sums over the internal degrees of freedom, the spins and isospins. Hence an estimate of an expectation value is obtained from:

$$\langle O\rangle = \frac{\int d\mathbf{R}\langle\Psi_T(\mathbf{R})|O|\Psi_T(\mathbf{R})\rangle}{\int d\mathbf{R}\langle\Psi_T(\mathbf{R})|\Psi_T(\mathbf{R})\rangle} \approx \frac{\sum_i \langle\Psi_T(\mathbf{R}_i)|O|\Psi_T(\mathbf{R}_i)\rangle/W(\mathbf{R}_i)}{\sum_i \langle\Psi_T(\mathbf{R}_i)|\Psi_T(\mathbf{R}_i)\rangle/W(\mathbf{R}_i)}, \qquad (24)$$

In the case of the Hamiltonian, we are averaging $\langle\Psi_T|H|\Psi_T\rangle/W$ (the "local" energy) over the points to yield an estimate of the ground-state energy.

Several variations on the standard methods are incorporated to treat light nuclei. First, instead of computing the full wave function $|\Psi_T\rangle$ in Eq. (16), one can sample over the order of pair and triplet correlation operators F_{ij} and F_{ijk} that are implied by the symmetrization operators $\mathcal{S}$ in Eq. (16). These orders must be sampled independently for the left and right hand wave functions and a positive definite choice made for a probability density $W(\mathbf{R})$.

In all cases, Monte Carlo methods are used to evaluate the coordinate space integrals, while spin-isospin sums are explicitly evaluated. The number of spin degrees of freedom grows as 2^A, while the isospin grows a little more slowly due to charge and (approximate) isospin conservation. The efficiency of the variational calculations can be dramatically improved by calculating energy differences between different wave functions. Nevertheless, these explicit spin-isospin summations require computing time that grows exponentially with A; a requirement that has limited standard VMC calculations of nuclear systems to light nuclei.

Once the variational parameters have been optimized, the expectation value of any ground-state observable can be evaluated using Eq. (24). Off-diagonal observables, such as momentum distributions, can be similarly evaluated. They simply require an additional integration variable corresponding to the off-diagonal displacement. Experimental quantities of interest include charge and magnetic form factors, sum rules, etc. In addition, other quantities can be computed that are not directly observable experimentally, but are useful in approximate theories of reactions, including momentum distributions of nucleons and nucleon clusters. A summary of some recent results is given below, additional results are presented in Refs. [4,52].

3.2 Green's function Monte Carlo

Diffusion or Green's function Monte Carlo (GFMC) methods rely upon the path-integral approach to evaluate the imaginary-time propagation of the wave function:

$$|\Psi_0\rangle = \lim_{\tau\to\infty} \exp[-(H-E_0)\tau]|\Psi_T\rangle \ , \tag{25}$$

where $|\Psi_0\rangle$ is the ground-state of H with energy E_0, and $|\Psi_T\rangle$ is a trial state. In order to evaluate this propagation, the imaginary-time τ is split up into small time slices $\Delta\tau$, and an equation of the form

$$|\Psi(\tau+\Delta\tau)\rangle = \exp[-(H-E_0)\Delta\tau]|\Psi(\tau)\rangle \tag{26}$$

is iterated.

This method has a long history, starting with calculations of the α-particle using a spin-isospin independent interaction by Kalos [54]. It has also been used extensively for problems in atomic and condensed matter physics. The first application to state-dependent interactions was provided by Carlson [55], and more realistic interactions were used in Refs. [56,57]. Recently calculations for A=6 and 7 have been performed, which are the first direct microscopic calculations of these p-shell nuclei [47,58].

The first element in performing such a calculation is the evaluation of the matrix elements of the short-time propagator:

$$\langle \mathbf{R}',\chi'|\exp(-H\Delta\tau)|\mathbf{R},\chi\rangle \equiv G(\mathbf{R}',\mathbf{R};\Delta\tau) \approx \left[\prod_{i=1,A} G_{0,i}(|\mathbf{r}_i'-\mathbf{r}_i|)\right]$$
$$\times \sum_{\chi_1,\chi_2} \langle\chi'|\left[1-\frac{\Delta\tau}{2}\sum_{i<j<k} V_{ijk}(\mathbf{R}')\right]|\chi_1\rangle\langle\chi_1|\mathcal{S}\prod_{i<j}\left[\frac{g_{ij}(\mathbf{r}_{ij}',\mathbf{r}_{ij})}{g_{0,ij}(\mathbf{r}_{ij}',\mathbf{r}_{ij})}\right]|\chi_2\rangle$$
$$\times\langle\chi_2|\left[1-\frac{\Delta\tau}{2}\sum_{i<j<k} V_{ijk}(\mathbf{R})\right]|\chi\rangle, \tag{27}$$

where the χ represent A-nucleon spin-isospin states, $G_{0,i}$ and $g_{0,ij}$ are the free one- and two-body imaginary-time propagators, respectively, and g_{ij} is the interacting two-body propagator.

The free propagators are simple Gaussians:

$$G_{0,i} = N_1 \exp\left[-m\frac{(\mathbf{r}_i'-\mathbf{r}_i)^2}{2\Delta\tau}\right] \ , \tag{28}$$

$$g_{0,ij} = N_2 \exp\left[-m\frac{(\mathbf{r}_{ij}'-\mathbf{r}_{ij})^2}{4\Delta\tau}\right] \ , \tag{29}$$

with normalizations N_i such that the norm of the flux is preserved ($\int d\mathbf{r}_i\, G_{0,i} = 1$). The pair propagator g_{ij} is the imaginary-time equivalent of the two-body T-matrix, it is a matrix in the two-body spin-isospin space and must be calculated numerically. The propagator satisfies an evolution equation:

$$\langle\chi_{ij}'|\left[\frac{\partial}{\partial\tau}+H_{ij}\right] g_{ij}(\mathbf{r}',\mathbf{r};\tau)|\chi_{ij}\rangle = 0 \ , \tag{30}$$

where

$$H_{ij} = -(1/m)\nabla_{ij}^2 + v_{ij} \ , \tag{31}$$

and χ_{ij} and χ_{ij}' are two-nucleon spin-isospin states. The g_{ij} also satisfy a boundary condition

$$\langle\chi_{ij}'|g_{ij}(\mathbf{r}',\mathbf{r};\tau{=}0)|\chi_{ij}\rangle = \delta(\mathbf{r}-\mathbf{r}')\delta_{\chi_{ij}',\chi_{ij}}. \tag{32}$$

Techniques for calculating and storing g_{ij} are described in detail in Ref. [58].

Once the propagator $G(\mathbf{R},\mathbf{R}';\Delta\tau)$ is constructed, a practical algorithm must be implemented to carry out the iteration of the wave function in Eq. (26). The scheme currently used for sampling the paths is described in detail in Ref. [58], here we simply sketch the basic ideas. Since the wave function (propagators) are vectors (matrices) in spin-isospin space, a scalar quantity must be defined to sample the paths. In principle, any set of paths can be chosen as long as the probability used to choose the paths is divided out when computing expectation values. To minimize the variance, though, it is important to follow as closely as possible standard importance sampling techniques used in traditional Green's function and diffusion Monte Carlo [58]. In essence, this requires sampling from a kernel so that the probability of a configuration at $\mathbf{R}$ is proportional to $\sum_\chi\langle\Psi_T(\mathbf{R})|\chi\rangle\langle\chi|\Psi(\mathbf{R};\tau)\rangle$. In the limit that the trial wave function Ψ_T is exact, and the propagator is sampled exactly, this method would produce the correct ground-state energy with no variance.

To this end, we introduce an importance function I that depends upon the full trial and GFMC wave functions. The calculations proceed by sampling paths from $I[\Psi_T(\mathbf{R}),\Psi(\mathbf{R};\tau)]$. The importance function must be real and positive and a convenient choice is:

$$I[\Psi_T(\mathbf{R}),\Psi(\mathbf{R};\tau)] = \left|\sum_\chi\langle\Psi_T(\mathbf{R})|\chi\rangle\langle\chi|\Psi(\mathbf{R};\tau)\rangle\right|$$
$$+\epsilon\sum_\chi\left|\langle\Psi_T(\mathbf{R})|\chi\rangle\langle\chi|\Psi(\mathbf{R};\tau)\rangle\right| \ , \tag{33}$$

where ϵ is a small positive coefficient. The second term ensures that all paths are allowed with a positive probability. In this equation and those that follow, the dependence upon the symmetrization $\mathcal{S}$ in the pair and triplet orders will be suppressed, both in the wave function, Eq. (16), and the propagator, Eq. (27). The pair and triplet orders are, in fact, sampled in both cases. Details of the sampling and weighting of paths are described in Ref. [58].

Branching techniques are used to split (delete) paths with large (small) importance functions $I[\Psi_T(\mathbf{R}), \Psi(\mathbf{R};\tau)]$ in a statistically unbiased manner. After branching, expectation values can be recovered from the equivalent of Eq. (24) evaluated between the trial and propagated GFMC wave functions:

$$\langle O(\tau)\rangle \approx \frac{\sum_i \langle \Psi_T(\mathbf{R}_i)|O|\Psi(\mathbf{R}_i;\tau)\rangle / I[\Psi_T(\mathbf{R}_i), \Psi(\mathbf{R}_i;\tau)]}{\sum_i \langle \Psi_T(\mathbf{R}_i)|\Psi(\mathbf{R}_i;\tau)\rangle / I[\Psi_T(\mathbf{R}_i), \Psi(\mathbf{R}_i;\tau)]} \quad . \tag{34}$$

This is the basis of the importance sampled GFMC algorithm for non-central interactions. Iterating this equation propagates the amplitudes of the wave function in a way designed to minimize statistical fluctuations in calculated expectation values.

The matrix element in Eq. (34) is a "mixed" estimate; it is of the form

$$\langle O\rangle_{\rm mix} = \frac{\langle \Psi_T|O\exp(-H\tau)|\Psi_T\rangle}{\langle \Psi_T|\exp(-H\tau)|\Psi_T\rangle} \quad . \tag{35}$$

The value $O_{\rm mix}$ is the matrix element of the trial (variational) and the true ground-state. The mixed estimate is sufficient to evaluate the ground-state energy, since the Hamiltonian commutes with the propagator. Indeed, an upper bound to the true ground-state energy E_0 is obtained for any value of τ:

$$\langle H\rangle_{\rm mix} = \frac{\langle \Psi_T|\exp(-H\tau/2)H\exp(-H\tau/2)|\Psi_T\rangle}{\langle \Psi_T|\exp(-H\tau/2)\exp(-H\tau/2)|\Psi_T\rangle} \geq E_0 \quad . \tag{36}$$

Of course, the actual convergence is governed by the accuracy of the trial wave function and the spectrum of the Hamiltonian. Often knowledge of the spectrum can be used to estimate the remaining error in a calculation that necessarily proceeds to only a finite τ.

For quantities other than the energy, one typically estimates the true ground-state expectation value by extrapolating from the mixed and variational estimates:

$$\langle O\rangle \approx 2\,\langle O\rangle_{\rm mix} - \frac{\langle \Psi_T|O|\Psi_T\rangle}{\langle \Psi_T|\Psi_T\rangle} \quad , \tag{37}$$

which is accurate to first order in the difference between Ψ and Ψ_T. The variational wave functions used in this work are typically quite accurate, so

this estimate is usually sufficient. For momentum-independent quantities, one can also retain a time history of the path in order to reconstruct an estimate of the form:

$$\langle O\rangle = \frac{\langle \Psi_T|\exp(-H\tau/2)O\exp(-H\tau/2)|\Psi_T\rangle}{\langle \Psi_T|\exp(-H\tau/2)\exp(-H\tau/2)|\Psi_T\rangle} \quad . \tag{38}$$

For momentum-dependent operators O, however, the statistical fluctuations associated with this estimate can be quite large.

Two caveats remain in present-day GFMC calculations of light nuclei. First, due to the well-known "sign-problem" in all path-integral simulations of fermions, the statistical error grows rapidly with τ. Present-day calculations are typically limited to τ of the order of $0.05-0.1$ MeV^{-1}. This is not as severe a situation as one might suppose, since we have quite accurate variational wave functions available for these nuclei and we have a significant knowledge of the excitation spectra in these systems. For calculations of six- and seven-body nuclei, it is useful to perform a shell-model like diagonalization in VMC to determine the optimum amplitudes for the various symmetry components of the p-wave part of the wave function [58]. Nevertheless, for some problems it may be quite useful to have a path-integral approximation which provides another type of approximation to the true ground-state. For example, the fixed-node [59,60] and constrained-path methods [61] have proven quite valuable in condensed matter problems. These constraints can often be relaxed to yield an even better estimate of observables.

The other concern is that in all currently available GFMC calculations, an approximate interaction which contains no $\mathbf{p}^2$ terms has been used in the propagation. Perturbation theory is then used to determine the expectation value of the difference between the two Hamiltonians. This approximation has proven to be quite accurate in studies of the three- and four-body systems. Although the equations above are still correct for an interaction with $\mathbf{p}^2$, $\mathbf{L}^2$ or $(\mathbf{L}\cdot\mathbf{S})^2$ interactions, a direct implementation of the method will yield large statistical errors. Again, variational schemes based upon constraints to the path-integral may prove useful.

GFMC has proven to be quite accurate in the three-, and now four-body systems in which it has been tested. Recent applications to larger systems [47,58] provide the first real tests of these microscopic models beyond A=4. It is also possible to compute low-energy scattering with path-integral techniques, as well as obtain information about a variety of dynamic nuclear response functions. A selection of results is presented in the following section.

3.3 *Spectra of the light nuclei*

The spectra of light nuclear systems provide the first test of nuclear interaction models: only if the spectra are well reproduced one can expect to accurately calculate other low energy and momentum observables, like radii, form factors, and scattering lengths.

A summary of VMC and GFMC results for the A=4-7 nuclei ground-state energies is given in Fig. 6. These results correspond to the Argonne v_{18} two-nucleon [5] and Urbana-IX three-nucleon [47] interactions. Note that the strength of the three-nucleon interaction is fixed by fitting the ^{3}H binding energy in a GFMC calculation, and the saturation density of nuclear matter in a variational calculation based on the Fermi-hypernetted-chain-summation technique.

4 The nuclear electromagnetic current operator

The simplest description of nuclei is based on a non-relativistic many-body theory of interacting nucleons. Within this framework, the nuclear electromagnetic current operators are expressed in terms of those associated with the individual protons and neutrons–the so-called impulse approximation (IA). Such a description, though, is certainly incomplete. The NN interaction is mediated, at large internucleon distances, by pion-exchange, and indeed seems to be well represented, even at short and intermediate distances, by meson exchange mechanisms, which naturally lead to effective many-body current operators. It should be realized that these many-body current operators arise, as does the NN interaction itself, as a consequence of the elimination of the mesonic degrees of freedom from the nuclear state vector. Clearly, such an approach is justified only at energies below the threshold for meson (specifically, pion) production, since above this threshold these non-nucleonic degrees of freedom have to be explicitly included in the state vector.

Two-body electromagnetic current operators have conventionally been derived as the non-relativistic limit of Feynman diagrams, in which the meson-baryon couplings have been obtained from either effective chiral Lagrangians [62] or semi-empirical models for the off-shell pion-nucleon amplitude [63]. These methods of constructing effective current operators, however, do not address the problem of how to model the composite structure of the hadrons in the phenomenological meson-baryon vertices. This structure is often parametrized in terms of form factors. For the electromagnetic case, however, gauge invariance actually puts constraints on these form factors by linking the divergence of the two-body currents to the commutator of the charge operator with the NN interaction. The latter contains form factors too, but these are determined phenomenologically by fitting NN data. Thus the continuity equation reduces the model dependence of the two-body currents by relating them to the form of the interaction. This point of view has been emphasized by Riska and collaborators [64–68] and others [69–71], and is adopted in the treatment of two-body currents that we discuss below.

The nuclear electromagnetic charge and current operators, respectively $\rho(\mathbf{q})$ and $\mathbf{j}(\mathbf{q})$, are expanded into a sum of one-, two-, and many-body terms that operate on the nucleon degrees of freedom:

$$\rho(\mathbf{q}) = \sum_i \rho_i^{(1)}(\mathbf{q}) + \sum_{i<j} \rho_{ij}^{(2)}(\mathbf{q}) + \cdots \ , \tag{39}$$

$$\mathbf{j}(\mathbf{q}) = \sum_i \mathbf{j}_i^{(1)}(\mathbf{q}) + \sum_{i<j} \mathbf{j}_{ij}^{(2)}(\mathbf{q}) + \cdots \ . \tag{40}$$

The one-body operators $\rho_i^{(1)}$ and $\mathbf{j}_i^{(1)}$ are obtained from the covariant single-nucleon current

$$j^\mu = \overline{u}(\mathbf{p}') \left[F_1(Q^2)\gamma^\mu + F_2(Q^2)\frac{i\sigma^{\mu\nu}q_\nu}{2m} \right] u(\mathbf{p}) \ , \tag{41}$$

where $\mathbf{p}$ ($\mathbf{p}'$) is the initial (final) momentum of the nucleon of mass m, and $F_1(Q^2)$ and $F_2(Q^2)$ are its Dirac and Pauli form factors taken as function of the four-momentum transfer $Q^2 = -q_\mu q^\mu > 0$, with $q_\mu = p'_\mu - p_\mu$. The Bjorken and Drell [72] convention is used for the γ-matrices, and $\sigma^{\mu\nu} = (i/2)\,[\gamma^\mu\,,\,\gamma^\nu]$. The j^μ is expanded in powers of $1/m$ and, including terms up to order $1/m^2$, the charge (μ=0) component can be written as

$$\rho_i^{(1)}(\mathbf{q}) = \rho_{i,\mathrm{NR}}^{(1)}(\mathbf{q}) + \rho_{i,\mathrm{RC}}^{(1)}(\mathbf{q}) \ , \tag{42}$$

with

$$\rho_{i,\mathrm{NR}}^{(1)}(\mathbf{q}) = \epsilon_i \, e^{i\mathbf{q}\cdot\mathbf{r}_i} \ , \tag{43}$$

$$\begin{aligned} \rho_{i,\mathrm{RC}}^{(1)}(\mathbf{q}) = & \left(\frac{1}{\sqrt{1+Q^2/4m^2}} - 1 \right) \epsilon_i \, e^{i\mathbf{q}\cdot\mathbf{r}_i} \\ & - \frac{i}{4m^2} \left(2\,\mu_i - \epsilon_i \right) \mathbf{q} \cdot (\boldsymbol{\sigma}_i \times \mathbf{p}_i) \, e^{i\mathbf{q}\cdot\mathbf{r}_i} \ , \end{aligned} \tag{44}$$

while the current components ($\mu = 1,2,3$) are expressed as

$$\mathbf{j}_i^{(1)}(\mathbf{q}) = \frac{1}{2m}\epsilon_i \left\{ \mathbf{p}_i \,,\, e^{i\mathbf{q}\cdot\mathbf{r}_i} \right\} - \frac{i}{2m}\mu_i \, \mathbf{q} \times \boldsymbol{\sigma}_i \, e^{i\mathbf{q}\cdot\mathbf{r}_i} \ , \tag{45}$$

where $\{\cdots,\cdots\}$ denotes the anticommutator. Here we have defined

$$\epsilon_i \equiv \frac{1}{2}\left[G_E^S(Q^2) + G_E^V(Q^2)\tau_{z,i}\right] \ , \tag{46}$$

$$\mu_i \equiv \frac{1}{2}\left[G_M^S(Q^2) + G_M^V(Q^2)\tau_{z,i}\right] \ , \tag{47}$$

and $\mathbf{p}$, σ, and τ are the nucleon's momentum, Pauli spin and isospin operators, respectively. The two terms proportional to $1/m^2$ in $\rho^{(1)}_{i,\rm RC}$ are the well known Darwin-Foldy and spin-orbit relativistic corrections[73,74], respectively.

The superscripts S and V of the Sachs form factors G_E and G_M denote, respectively, isoscalar and isovector combinations of the proton and neutron electric and magnetic form factors[75]. The G_E and G_M are related to the Dirac and Pauli form factors in Eq. (41) via:

$$G_E(Q^2) = F_1(Q^2) - \frac{Q^2}{4m^2}F_2(Q^2) \ , \tag{48}$$

$$G_M(Q^2) = F_1(Q^2) + F_2(Q^2) \ , \tag{49}$$

and are normalized so that

$$G_E^S(Q^2{=}0) = G_E^V(Q^2{=}0) = 1 \ , \tag{50}$$

$$G_M^S(Q^2{=}0) = \mu_p + \mu_n = 0.880\,\mu_N \ , \tag{51}$$

$$G_M^V(Q^2{=}0) = \mu_p - \mu_n = 4.706\,\mu_N \ , \tag{52}$$

where μ_p and μ_n are the magnetic moments of the proton and neutron in terms of the nuclear magneton μ_N. The Q^2-dependence of the Sachs form factors is determined by fitting electron-nucleon scattering data[76–79]. The proton electric and magnetic form factors are experimentally fairly well known over a wide range of momentum transfers[78,80–83]. In contrast, the present data on the neutron form factors[84–87], particularly the electric one, are obtained from model-dependent analyses of $e\,d$ scattering, and the available semi-empirical parametrizations for them differ widely, particularly at high momentum transfers. Until this uncertainty in the detailed behavior of the electromagnetic form factors of the nucleon is narrowed, quantitative predictions of electro-nuclear observables at high momentum transfers will remain rather tentative.

The electromagnetic current operator must satisfy the continuity equation

$$\mathbf{q}\cdot\mathbf{j}(\mathbf{q}) = [H\,,\,\rho(\mathbf{q})] \ , \tag{53}$$

where the Hamiltonian H includes two- and three-nucleon interactions

$$H = \sum_i \frac{\mathbf{p}_i^2}{2m} + \sum_{i<j} v_{ij} + \sum_{i<j<k} V_{ijk} \ . \tag{54}$$

To lowest order in $1/m$, the continuity equation (53) separates into separate continuity equations for the one-, two-, and many-body current operators

$$\mathbf{q}\cdot\mathbf{j}_i^{(1)}(\mathbf{q}) = \left[\frac{\mathbf{p}_i^2}{2m}\,,\,\rho^{(1)}_{i,\rm NR}(\mathbf{q})\right] \ , \tag{55}$$

$$\mathbf{q}\cdot\mathbf{j}_{ij}^{(2)}(\mathbf{q}) = \left[v_{ij}\,,\,\rho^{(1)}_{i,\rm NR}(\mathbf{q}) + \rho^{(1)}_{j,\rm NR}(\mathbf{q})\right] \ , \tag{56}$$

and a similar equation involving three-nucleon currents and interactions.

The one-body current in Eq. (45) is easily shown to satisfy Eq. (55). The isospin- and momentum-dependence of the two- and three-nucleon interactions, however, lead to non-vanishing commutators with the non-relativistic one-body charge operator, and thus link the longitudinal part of the corresponding two- and three-body currents to the form of these interactions. Here we will limit our discussion to two-body currents; a recent investigation of three-body current operators is presented in Ref.[88].

4.1 Electromagnetic two-body current operators from the two-nucleon interaction

All realistic NN interactions include isospin-dependent central, spin-spin and tensor components

$$\left[v^\tau(r_{ij}) + v^{\sigma\tau}(r_{ij})\sigma_i\cdot\sigma_j + v^{t\tau}(r_{ij})S_{ij}\right]\tau_i\cdot\tau_j \ , \tag{57}$$

where the $\sigma\tau$ and $t\tau$ terms include the long-range one-pion-exchange potential (OPEP). The $\tau_i\cdot\tau_j$ operator, which does not commute with the charge operators in Eq. (56), is formally equivalent to an implicit momentum dependence[89]. This is shown by considering the product of space-, spin-, and isospin-exchange operators, denoted respectively as E_{ij}, E^σ_{ij}, E^τ_{ij}, where

$$\mathrm{E}_{ij} = \exp\left[\mathrm{i}\int_{r_i}^{r_j} d\mathbf{s}\cdot(\mathbf{p}_i - \mathbf{p}_j)\right] \ , \tag{58}$$

$$\mathrm{E}^\sigma_{ij} = \frac{1+\sigma_i\cdot\sigma_j}{2} \ , \tag{59}$$

$$\mathrm{E}^\tau_{ij} = \frac{1+\tau_i\cdot\tau_j}{2} \ . \tag{60}$$

They must satisfy $E_{ij}\,E^{\sigma}_{ij}\,E^{\tau}_{ij} = -1$. The line integral in Eq. (58) is along any path leading from $\mathbf{r}_i$ to $\mathbf{r}_j$. Thus two-body current operators associated with the $\tau_i \cdot \tau_j$-dependent interactions, Eq. (57), could be constructed by minimal substitution in the space-exchange operator:

$$\mathbf{p}_i \rightarrow \mathbf{p}_i - e_i\,\mathbf{A}(\mathbf{r}_i)\ , \tag{61}$$

where $\mathbf{A}(\mathbf{r}_i)$ is the vector potential. Due to the arbitrariness of the integration path in Eq. (58), such a prescription does not lead, however, to unique two-body currents [90]. Therefore, an assumption has to be made about the dynamical origin of the interactions in Eq. (57) in order to construct the associated currents.

At intermediate and large internucleon separation distances, the v^{τ}, $v^{\sigma\tau}$, and $v^{t\tau}$ interactions are assumed to be due to π- and ρ-meson exchanges. The πNN and ρNN coupling Lagrangians are given by:

$$L_{\pi NN}(x) = \frac{f_{\pi NN}}{m_\pi}\overline{\psi}(x)\gamma^\mu\gamma_5\tau\psi(x)\cdot\partial_\mu\pi(x)\ , \tag{62}$$

$$L_{\rho NN}(x) = g_{\rho NN}\overline{\psi}(x)\left[\left(\gamma^\mu + \frac{\kappa_\rho}{2m}\sigma^{\mu\nu}\partial_\nu\right)\rho_\mu(x)\right]\cdot\tau\psi(x)\ , \tag{63}$$

where $\pi(x)$ and $\rho(x)$ are the π- and ρ-meson T=1 fields, $\psi(x)$ is the T=1/2 nucleon field, m_π and m_ρ are the meson masses, $f_{\pi NN}$, $g_{\rho NN}$ and κ_ρ are the pseudo-vector πNN, and the vector and tensor ρNN coupling constants ($f^2_{\pi NN}/4\pi$=0.075, $g^2_{\rho NN}/4\pi$=0.55, and κ_ρ=6.6), respectively. By performing a non-relativistic reduction of the one-boson-exchange Feynman amplitudes, the π- and ρ-meson exchange interactions are obtained in momentum space as

$$\left[v_{\rho S}(k) + \left[v_\pi(k) + 2\,v_\rho(k)\right]k^2\sigma_i\cdot\sigma_j - \left[v_\pi(k) - v_\rho(k)\right]S_{ij}(\mathbf{k})\right]\tau_i\cdot\tau_j\ , \tag{64}$$

where

$$v_{\rho S}(k) \equiv g^2_{\rho NN}\frac{1}{k^2+m^2_\rho}\ , \tag{65}$$

$$v_\pi(k) \equiv -\frac{f^2_{\pi NN}}{3m^2_\pi}\frac{1}{k^2+m^2_\pi}\ , \tag{66}$$

$$v_\rho(k) \equiv -\frac{g^2_{\rho NN}}{12m^2}\frac{(1+\kappa_\rho)^2}{k^2+m^2_\rho}\ . \tag{67}$$

The tensor operator in momentum space is defined as

$$S_{ij}(\mathbf{k}) = k^2\sigma_i\cdot\sigma_j - 3\,\sigma_i\cdot\mathbf{k}\,\sigma_j\cdot\mathbf{k}\ . \tag{68}$$

The isovector two-body currents corresponding to π- and ρ-meson exchanges can be derived by minimal substitution $\partial_\mu \rightarrow \partial_\mu \pm iA_\mu(x)$ in the πNN and ρNN coupling Lagrangians, Eqs. (62)-(63), and in the free π- and ρ-meson Lagrangians:

$$L_\pi(x) = \frac{1}{2}\partial_\mu\pi(x)\cdot\partial^\mu\pi(x) - \frac{m^2_\pi}{2}\pi(x)\cdot\pi(x)\ , \tag{69}$$

$$L_\rho(x) = -\frac{1}{4}\left[\partial_\mu\rho_\nu(x) - \partial_\nu\rho_\mu(x)\right]\cdot\left[\partial^\mu\rho^\nu(x) - \partial^\nu\rho^\mu(x)\right] - \frac{m^2_\rho}{2}\rho^\mu(x)\cdot\rho_\mu(x)\ . \tag{70}$$

The non-relativistic reduction of the Feynman amplitudes shown in Fig. 7 leads to the momentum-space two-body operators:

$$\mathbf{j}^{(2)}_{ij,\pi}(\mathbf{k}_i,\mathbf{k}_j) = 3\mathrm{i}(\tau_i\times\tau_j)_z\,G^V_E(Q^2)\left[v_\pi(k_j)\sigma_i(\sigma_j\cdot\mathbf{k}_j) - v_\pi(k_i)\sigma_j(\sigma_i\cdot\mathbf{k}_i) + \frac{\mathbf{k}_i-\mathbf{k}_j}{k^2_i-k^2_j}\left[v_\pi(k_i)-v_\pi(k_j)\right](\sigma_i\cdot\mathbf{k}_i)(\sigma_j\cdot\mathbf{k}_j)\right]\ , \tag{71}$$

$$\begin{aligned}\mathbf{j}^{(2)}_{ij,\rho}(\mathbf{k}_i,\mathbf{k}_j) = -3\mathrm{i}(\tau_i\times\tau_j)_z\,G^V_E(Q^2)\Big[&v_\rho(k_j)\sigma_i\times(\sigma_j\times\mathbf{k}_j) \\ &-v_\rho(k_i)\sigma_j\times(\sigma_i\times\mathbf{k}_i) - \frac{v_\rho(k_i)-v_\rho(k_j)}{k^2_i-k^2_j} \\ &\left[(\mathbf{k}_i-\mathbf{k}_j)(\sigma_i\times\mathbf{k}_i)\cdot(\sigma_j\times\mathbf{k}_j)\right. \\ &\left.+(\sigma_i\times\mathbf{k}_i)\,\sigma_j\cdot(\mathbf{k}_i\times\mathbf{k}_j) + (\sigma_j\times\mathbf{k}_j)\,\sigma_i\cdot(\mathbf{k}_i\times\mathbf{k}_j)\right] \\ &+\frac{\mathbf{k}_i-\mathbf{k}_j}{k^2_i-k^2_j}\left[v_{\rho S}(k_i)-v_{\rho S}(k_j)\right]\Big]\ ,\end{aligned} \tag{72}$$

where $\mathbf{k}_i$ and $\mathbf{k}_j$ are the fractional momenta delivered to nucleons i and j with $\mathbf{q} = \mathbf{k}_i + \mathbf{k}_j$, and the form factor $G^V_E(Q^2)$ has been included to take into account

the electromagnetic structure of the nucleon. The continuity equation requires that the same form factor be used to describe the electromagnetic structure of the hadrons in the longitudinal part of the current operator and in the charge operator. Again, it places no restrictions on the electromagnetic form factors which may be used in the transverse parts of the current. Ignoring this ambiguity, the choice made here ($G_E^V(Q^2)$) satisfies the "minimal" requirement of current conservation. However, for a somewhat different discussion of this point we refer the reader to Ref. [91].

The first two terms in Eqs. (71)–(72) are seagull currents corresponding to diagrams (a) and (b) of Fig. 7, while the remaining terms are the currents due to π- and ρ-meson in flight. These operators with the $v_\pi(k)$, $v_\rho(k)$, and $v_{\rho S}(k)$ propagators suitably modified by the inclusion of form factors have commonly been used in the investigation of exchange current effects in nuclei. A first systematic derivation of pion and heavy meson exchange current operators was in fact given by Chemtob and Rho in their seminal 1971 paper [63]. While these simple two-body currents satisfy the continuity equation with the corresponding meson exchange interactions, they do not satisfy the continuity equation with the realistic models for the NN interaction that are used to construct nuclear wave functions. A method of obtaining current operators which satisfy the continuity equation for any given v^τ, $v^{\sigma\tau}$, and $v^{t\tau}$ interactions has been proposed by Riska [65] and, independently, Arenhovel *et al.* [69]. In this method these interactions are attributed to exchanges of families of π-like pseudoscalar (PS) and ρ-like vector (V) mesons. The sum of all T=1 PS- and V-exchange terms is then obtained as

$$v_{PS}(k) = \left[v^{\sigma\tau}(k) - 2\,v^{t\tau}(k)\right]/3 \ , \tag{73}$$

$$v_V(k) = \left[v^{\sigma\tau}(k) + v^{t\tau}(k)\right]/3 \ , \tag{74}$$

$$v_{VS}(k) = v^{\tau}(k) \ , \tag{75}$$

where

$$v^{\tau}(k) = 4\pi \int_0^\infty r^2 dr\, j_0(kr) v^{\tau}(r) \ , \tag{76}$$

$$v^{\sigma\tau}(k) = \frac{4\pi}{k^2} \int_0^\infty r^2 dr\, \left[j_0(kr) - 1\right] v^{\sigma\tau}(r) \ , \tag{77}$$

$$v^{t\tau}(k) = \frac{4\pi}{k^2} \int_0^\infty r^2 dr\, j_2(kr) v^{t\tau}(r) \ . \tag{78}$$

The expression for $v^{\sigma\tau}(k)$ reflects the fact that in all NN interaction models derived from a relativistic scattering amplitude a δ-function term has been

dropped from the spin-spin component. The current operators $\mathbf{j}^{(2)}_{ij,PS}$ and $\mathbf{j}^{(2)}_{ij,V}$, obtained by using $v_{PS}(k)$, $v_V(k)$, and $v_{VS}(k)$ in place of $v_\pi(k)$, $v_\rho(k)$, and $v_{\rho S}(k)$ in Eqs. (71)–(72) satisfy the continuity equation with the v^τ, $v^{\sigma\tau}$ and $v^{t\tau}$ potentials in the model interaction used to fit the NN scattering data, and to calculate nuclear ground- and scattering-state wave functions. In particular, there is no ambiguity left as to the proper form of the short-range behavior of the two-body current operator, as this is determined by the interaction model. Configuration-space expressions may be obtained from:

$$\mathbf{j}^{(2)}_{ij,a}(\mathbf{q}) = \int d\mathbf{x}\, e^{i\mathbf{q}\cdot\mathbf{x}} \int \frac{d\mathbf{k}_i}{(2\pi)^3} \frac{d\mathbf{k}_j}{(2\pi)^3} e^{i\mathbf{k}_i\cdot(\mathbf{r}_i-\mathbf{x})} e^{i\mathbf{k}_j\cdot(\mathbf{r}_j-\mathbf{x})} \mathbf{j}^{(2)}_{ij,a}(\mathbf{k}_i,\mathbf{k}_j) \ , \tag{79}$$

where a=PS or V, and are given explicitly in Ref. [92].

Although the Riska prescription obviously cannot be unique, it has nevertheless been shown to provide, at low and moderate values of momentum transfer (typically, below $\simeq$ 1 GeV/c), a satisfactory description of most observables where isovector two-body currents play a large (if not dominant) role, such as the deuteron threshold electro-disintegration [69,93], the neutron and proton radiative captures on proton [93] and deuterons [94] at low energies, and the magnetic moments and form factors of the trinucleons [92,95].

In addition to spin-spin and tensor components, all realistic interactions contain spin-orbit and quadratic momentum-dependent terms. The construction of the associated two-body current operators is less straightforward. A procedure similar to that used above to derive the π-like and ρ-like currents has been generalized to the case of the two-body currents from the spin-orbit interactions [96]. It consists, in essence, of attributing these to exchanges of σ-like and ω-like mesons for the isospin-independent terms, and to ρ-like mesons for the isospin-dependent ones. The explicit form of the resulting currents as well as their derivation can be found in the original reference [96].

The quadratically momentum-dependent terms represent, on the one hand, relativistic corrections to the central and spin-orbit interactions, which are proportional to $\mathbf{p}^2$ (p is the relative momentum) and, on the other hand, quadratic spin-orbit interactions. To construct the associated two-body current operators is, in general, difficult or impossible, because of the many approximations typically used to simplify the structure of these interaction components. Furthermore, some interactions, such as the Argonne models [5,9], contain terms proportional to $\mathbf{L}^2$, which do not appear in any natural way in boson-exchange models. Hence, in view of the fact that the numerical significance of these operators is anyway small, the two-body currents associated with the quadratic momentum-dependence are obtained by minimal substitution, Eq. (61), into

the corresponding interaction components[92].

The currents associated with the momentum dependence of the interaction are fairly short ranged, and have both isoscalar and isovector terms. Their contribution to isovector observables is found to be numerically much smaller than that due to the leading π-like current [92,95]. However, they give non-negligible corrections to isoscalar observables, such as the deuteron magnetic moment and $B(Q)$-structure function [5,93], and isoscalar combination of the magnetic moments and form factors of the trinucleons[92,95], as will be reported later in Sec. 5.2.

4.2 "Model-dependent" electromagnetic two-body current operators

The two-body currents discussed in the previous section are constrained by the continuity equation and do not contain any free parameters, since they are determined directly from the NN interaction. They can therefore be viewed as "model independent". There are, however, additional two-body currents which are purely transverse. These will be referred to as "model-dependent" two-body currents.

The class of model-dependent currents that has been considered in the literature contains two-body operators associated with electromagnetic transition couplings between different mesons, such as the $\rho\pi\gamma$ and $\omega\pi\gamma$ mechanisms, or with excitation of intermediate nucleon resonances (specifically, the Δ-isobar). These are found to be numerically much less important than the two-body currents from the v_8 part of the NN interaction, and will not be discussed further here; for a review, however, see Ref. [1].

4.3 Electromagnetic two-body charge operators

Several uncertainties arise when considering the two-body charge operator, in contrast to the two-body current operator. While the main parts of the two-body current are linked to the form of the NN interaction through the continuity equation, the most important two-body charge operators are model dependent and may be viewed as relativistic corrections. Until a systematic method for a simultaneous non-relativistic reduction of both the interaction and the electromagnetic current operator is developed, the definite form of the two-body charge operators remains uncertain, and one has to rely on perturbation theory.

Two-body charge operators fall into two classes. The first includes those effective operators that represent non-nucleonic degrees of freedom, such as nucleon-antinucleon pairs or nucleon-resonances, and which arise when those degrees of freedom are eliminated from the state vector. To the second class

belong those dynamical exchange charge effects that would appear even in a description explicitly including non-nucleonic excitations in the state vector. In a description based on meson exchange mechanisms these involve electromagnetic transition couplings between different mesons. The proper forms of the former operators depend on the method of eliminating the non-nucleonic degrees of freedom, and therefore evaluating their matrix elements with the usual non-relativistic nuclear wave functions represents only the first approximation to a systematic reduction [97]. We shall first consider the two-body charge operators of this class, to which belongs the long range pion-exchange charge operator.

The two-body charge operator due to pion exchange is derived by considering the low energy limit of the relativistic Born diagrams associated with the virtual pion photoproduction amplitude[62]. When these are evaluated with pseudovector pion-nucleon coupling, the following operator is obtained for diagram (a) of Fig. 8:

$$\begin{aligned} &\frac{1}{2}[F_1^S(Q^2)+F_1^V(Q^2)\tau_{z,i}]\frac{1}{E_{\rm in}-E}v_{ij,\pi}(\mathbf{k}_j) \\ &+\frac{f_{\pi NN}^2}{2mm_\pi^2}\frac{1}{2}[F_1^S(Q^2)+F_1^V(Q^2)\tau_{z,i}]\tau_i\cdot\tau_j\frac{\sigma_i\cdot\mathbf{q}\,\sigma_j\cdot\mathbf{k}_j}{m_\pi^2+k_j^2} \\ &+O(E_{\rm in}-E)\,; \end{aligned} \tag{80}$$

a similar operator corresponds to the time ordering in diagram (b) of Fig. 8. Here $\mathbf{q}$ is the momentum transfer to the nucleus, $\mathbf{k}_j$ the momentum transferred by the pion to nucleon j, and $E_{\rm in}$ and E are the energies of the initial and intermediate states, respectively. In Eq. (80) $v_{ij,\pi}(\mathbf{k}_j)$ is the OPEP in momentum space

$$v_{ij,\pi}(\mathbf{k}) = 3\,v_\pi(k)\tau_i\cdot\tau_j\,\sigma_i\cdot\mathbf{k}\,\sigma_j\cdot\mathbf{k}\,. \tag{81}$$

The first term in Eq. (80) contains the intermediate state Green's function and OPEP. It is therefore contained in the bound state matrix elements of the single-nucleon charge operator (i.e., in the impulse approximation). The second term represents, however, a part of the exchange charge operator. There is an additional contribution due to the energy dependence of the pion propagator[27,97,98]. To these operators, one must add that associated with the direct coupling of the photon to the exchanged pion [27,97,98]. However, this latter operator as well as that due to retardation effects in the pion propagator give rise to non-local isovector contributions which are expected to provide only small corrections to the leading local term, and have typically been neglected in studies of charge exchange effects in nuclei. For example, in the few-nucleon

systems these operators would only contribute to the isovector combination of the ^{3}He and ^{3}H charge form factors, which is anyway a factor of three smaller than the isoscalar. Thus the two-body charge operator due to pion exchange is simply taken as

$$\rho_{ij,\pi}(\mathbf{k}_i,\mathbf{k}_j) = -\frac{3}{2m}\Big[\left[F_1^S(Q^2)\tau_i\cdot\tau_j + F_1^V(Q^2)\tau_{z,j}\right] v_\pi(k_j)\sigma_i\cdot\mathbf{q}\,\sigma_j\cdot\mathbf{k}_j + \left[F_1^S(Q^2)\tau_i\cdot\tau_j + F_1^V(Q^2)\tau_{z,i}\right] v_\pi(k_i)\sigma_i\cdot\mathbf{k}_i\,\sigma_j\cdot\mathbf{q}\Big] \ , \quad (82)$$

where $\mathbf{k}_i + \mathbf{k}_j = \mathbf{q}$.

The effect of the pion exchange charge operator is enhanced by the similar operator that is associated with ρ-meson exchange. The ρ-meson exchange charge operator can be derived in the same way as the pion exchange charge operator by considering the non-relativistic reduction of the virtual ρ-meson photoproduction amplitudes in two-body diagrams of the form in Fig. 8, and eliminating the singular term that represents an iteration of the wave function. The form of the resulting operator is[62]

$$\rho_{ij,\rho}(\mathbf{k}_i,\mathbf{k}_j) = -\frac{3}{2m}\Big[\left[F_1^S(Q^2)\tau_i\cdot\tau_j + F_1^V(Q^2)\tau_{z,j}\right] v_\rho(k_j)(\sigma_i\times\mathbf{q})\cdot(\sigma_j\times\mathbf{k}_j) + \left[F_1^S(Q^2)\tau_i\cdot\tau_j + F_1^V(Q^2)\tau_{z,i}\right] v_\rho(k_i)(\sigma_j\times\mathbf{q})\cdot(\sigma_i\times\mathbf{k}_i)\Big] \ , \quad (83)$$

where again non-local terms and/or terms proportional to powers of $1/(1+\kappa_\rho)$ have been neglected. Due to its short range, the contribution associated with this operator is typically an order of magnitude smaller than that due to pion exchange.

The π- and ρ-meson exchange charge operators contain coupling constants and bare meson propagators, which are usually modified by *ad hoc* vertex form factors in order to take into account the finite extent of the nucleons. However, this model-dependence can be eliminated by replacing v_π and v_ρ with the v_{PS} and v_V defined in Eqs. (73)–(74). These replacements are the ones required for the construction of a two-body current operator that satisfies the continuity equation. It is reasonable to apply them to the two-body charge operators as the generalized meson propagators constructed in this way take into account the nucleon structure in a way consistent with the NN interaction. An additional reason for using the present construction is that it has been

shown to lead to predictions for the magnetic form factors of the trinucleons that are in good agreement with the experimental data[92,95].

All the exchange charge operators shown above belong to the first class of exchange operators, and appear as non-singular seagull terms in the non-relativistic reduction of the virtual photoproduction amplitudes for the exchanged mesons. The exchange charge operators that correspond to the $\rho\pi\gamma$ and $\omega\pi\gamma$ couplings belong to the (second) class of genuine dynamical exchange operators, those with transverse four-vector currents. Their contributions are found to be numerically very small at momentum transfers below 1 GeV/c. A discussion of them can be found in Ref.[1].

5 Electromagnetic structure of ground- and low-energy states of A=3–6 nuclei

In this section we give an overview of the current status of elastic and inelastic electromagnetic form factor calculations in the A=3–6 nuclei. Our discussion will be in the context of a unified approach to nuclear dynamics based on realistic two- and three-nucleon interactions and consistent two-body charge and current operators, those discussed in the previous section.

5.1 Elastic and inelastic electron scattering from nuclei: a review

In the one-photon-exchange approximation the electron scattering cross section involving a transition from an initial nuclear state $|J_i\rangle$ of spin J_i and rest mass m_i to a final nuclear state $|J_f\rangle$ of spin J_f, rest mass m_f and recoiling energy E_f can be expressed in the laboratory frame as[73,99]

$$\frac{d\sigma}{d\Omega} = 4\pi\sigma_M f_{\rm rec}^{-1}\Big[v_L F_L(q) + v_T F_T(q)\Big] \ , \quad (84)$$

where

$$\sigma_M = \left(\frac{\alpha\cos\theta/2}{2\epsilon_i\sin^2\theta/2}\right)^2 \ , \quad (85)$$

$$v_L = \frac{Q^4}{q^4} \ , \quad (86)$$

$$v_T = \tan^2\frac{\theta}{2} + \frac{Q^2}{2q^2} \ , \quad (87)$$

and the recoil factor $f_{\rm rec}$ is given by

$$f_{\rm rec} = 1 + \frac{\epsilon_f - \epsilon_i \cos\theta}{E_f} \simeq 1 + \frac{2\epsilon_i}{m_i} \sin^2\frac{\theta}{2} \ . \tag{88}$$

The electron kinematical variables are defined in Fig. 9. The last expression for $f_{\rm rec}$ in Eq. (88) is obtained by neglecting terms of order $(\omega/m_i)^2$ and higher, where

$$\frac{\omega}{m_i} = \frac{Q^2 + m_f^2 - m_i^2}{2m_i^2} \ . \tag{89}$$

The nuclear structure information is contained in the longitudinal and transverse form factors denoted, respectively, by $F_L(q)$ and $F_T(q)$. By fixing q and ω and varying θ it is possible to separate $F_L(q)$ from $F_T(q)$ in a procedure known as a Rosenbluth separation. Alternatively, by working at θ=180° one ensures that only the transverse form factor contributes to the cross section and so may be isolated (in this case, we observe that the combination $\sigma_M \tan^2\theta/2 \to (\alpha/2\epsilon_i)^2$ as $\theta \to 180°$, and is therefore finite in this limit).

The longitudinal and transverse form factors are expressed in terms of reduced matrix elements of Coulomb, electric, and magnetic multipole operators as[73,99]

$$F_L(q) = \frac{1}{2J_i+1} \sum_{J=0}^{\infty} |\langle J_f \| T_J^{\rm Coul}(q) \| J_i \rangle|^2 \ , \tag{90}$$

$$F_T(q) = \frac{1}{2J_i+1} \sum_{J=1}^{\infty} \left[|\langle J_f \| T_J^{\rm El}(q) \| J_i \rangle|^2 + |\langle J_f \| T_J^{\rm Mag}(q) \| J_i \rangle|^2 \right] \ , \tag{91}$$

where we have defined

$$T_{JM}^{\rm Coul}(q) \equiv \int d\mathbf{x}\, j_J(qx)\, Y_{JM}(\hat{\mathbf{x}}) \rho(\mathbf{x}) \ , \tag{92}$$

$$T_{JM}^{\rm El}(q) \equiv \frac{1}{q} \int d\mathbf{x} \left[\nabla \times j_J(qx) \mathbf{Y}_{JJ_1}^M(\hat{\mathbf{x}}) \right] \cdot \mathbf{j}(\mathbf{x}) \ , \tag{93}$$

$$T_{JM}^{\rm Mag}(q) \equiv \int d\mathbf{x}\, j_J(qx)\, \mathbf{Y}_{JJ_1}^M(\hat{\mathbf{x}}) \cdot \mathbf{j}(\mathbf{x}) \ , \tag{94}$$

with

$$\mathbf{Y}_{JL1}^M(\hat{\mathbf{x}}) \equiv \sum_{M_L,\mu} \langle LM_L, 1\mu | JM \rangle Y_{LM_L}(\hat{\mathbf{x}})\, \hat{\mathbf{e}}_\mu \ , \tag{95}$$

$\hat{\mathbf{e}}_0 \equiv \hat{\mathbf{e}}_z$, and $\hat{\mathbf{e}}_{\pm 1} \equiv \mp(\hat{\mathbf{e}}_x \pm i\hat{\mathbf{e}}_y)/\sqrt{2}$. Here $\rho(\mathbf{x})$ and $\mathbf{j}(\mathbf{x})$ are the nuclear charge and current density operators, and $j_J(qx)$ are spherical Bessel functions. The

reduced matrix elements in Eqs. (90)-(91) are related to the matrix elements of the Fourier transforms $\rho(\mathbf{q})$ and $\mathbf{j}(\mathbf{q})$, introduced in Sec. 4, via[73]:

$$\langle J_f M_f | \rho(\mathbf{q}) | J_i M_i \rangle = 4\pi \sum_{J=0}^{\infty} \sum_{M=-J}^{J} i^J Y_{JM}^*(\hat{\mathbf{q}}) \frac{\langle J_i M_i, JM | J_f M_f \rangle}{\sqrt{2J_f+1}} \langle J_f \| T_J^{\rm Coul}(q) \| J_i \rangle \ , \tag{96}$$

$$\langle J_f M_f | \hat{\mathbf{e}}_\lambda(\mathbf{q}) \cdot \mathbf{j}(\mathbf{q}) | J_i M_i \rangle = -\sqrt{2\pi} \sum_{J=1}^{\infty} \sum_{M=-J}^{J} i^J \sqrt{2J+1}\, \mathcal{D}_{\lambda M}^J(0\,\theta_q\,0) \frac{\langle J_i M_i, JM | J_f M_f \rangle}{\sqrt{2J_f+1}} \left[\lambda \langle J_f \| T_J^{\rm Mag}(q) \| J_i \rangle + \langle J_f \| T_J^{\rm El}(q) \| J_i \rangle \right] \ , \tag{97}$$

where $\lambda = \pm 1$, $\hat{\mathbf{e}}_\lambda(\mathbf{q})$ are the spherical components of the virtual photon transverse polarization vector, and the $\mathcal{D}_{\lambda M}^J$ are standard rotation matrices. The expressions above correspond to the virtual photon being absorbed at an angle θ_q with respect to the quantization axis of the nuclear spins. The more familiar expressions for the multipole expansion of the charge and current matrix elements are recovered by taking q along the spin quantization axis, so that $Y_{JM}^*(\hat{\mathbf{q}}) \to \delta_{M,0}\sqrt{2J+1}/\sqrt{4\pi}$ and $\mathcal{D}_{\lambda M}^J(0\,\theta_q\,0) \to \delta_{\lambda,M}$.

It is useful to consider the parity and time-reversal properties of the multipole operators[73]. Thus the scalar and polar vector character of, respectively, the charge and current density operators under parity transformations implies that $T_{JM}^{\rm Coul}$ and $T_{JM}^{\rm El}$ have parity $(-1)^J$, while $T_{JM}^{\rm Mag}$ has parity $(-1)^{J+1}$. The resulting selection rules are $\pi_i\pi_f = (-1)^J$ ($\pi_i\pi_f = (-1)^{J+1}$) for Coulomb and electric (magnetic) transitions, where π_i and π_f are the parities of the initial and final states.

The Hermitian character of the operators $\rho(\mathbf{x})$ and $\mathbf{j}(\mathbf{x})$ as well as their transformation properties under time-reversal, $\rho(\mathbf{x}) \to \rho(\mathbf{x})$ and $\mathbf{j}(\mathbf{x}) \to -\mathbf{j}(\mathbf{x})$, can be shown to lead to the following relations:

$$\langle J_f \| T_J^{\rm Coul}(q) \| J_i \rangle = (-1)^{J_f+J-J_i} \langle J_i \| T_J^{\rm Coul}(q) \| J_f \rangle \ , \tag{98}$$

$$\langle J_f \| T_J^{\rm El,Mag}(q) \| J_i \rangle = (-1)^{J_f+J-J_i+1} \langle J_i \| T_J^{\rm El,Mag}(q) \| J_f \rangle \ . \tag{99}$$

These relations along with the parity selection rules stated above require, in particular, that elastic transitions, for which J_f=J_i, can only be induced by even-J Coulomb and odd-J magnetic multipole operators.

Finally, in the low-q or long-wavelength limit, the multipole operators defined above can be shown to behave as [73,99]

$$T^{\rm Coul}_{JM}(q) \simeq \sqrt{\frac{2J+1}{4\pi}}\frac{q^J}{(2J+1)!!}Q_{JM} \ , \tag{100}$$

$$Q_{JM} \equiv \sqrt{\frac{4\pi}{2J+1}}\int dx\, x^J Y_{JM}(\hat{x})\,\rho(x) \ , \tag{101}$$

$$T^{\rm Mag}_{JM}(q) \simeq -\frac{1}{i}\sqrt{\frac{2J+1}{4\pi}}\sqrt{\frac{J+1}{J}}\frac{q^J}{(2J+1)!!}\mu_{JM} \ , \tag{102}$$

$$\mu_{JM} \equiv \sqrt{\frac{4\pi}{2J+1}}\frac{1}{J+1}\int dx\,[x\times j(x)]\cdot\nabla\,[x^J Y_{JM}(\hat{x})] \ , \tag{103}$$

and

$$\begin{aligned} T^{\rm El}_{JM}(q) &\simeq \frac{1}{i}\sqrt{\frac{J+1}{J}}\frac{q^{J-1}}{(2J+1)!!}\int dx\, x^J Y_{JM}(\hat{x})\,\nabla\cdot j(x) \\ &= -\sqrt{\frac{2J+1}{4\pi}}\sqrt{\frac{J+1}{J}}\frac{m_f-m_i}{q}\frac{q^J}{(2J+1)!!}Q_{JM} \ , \end{aligned} \tag{104}$$

where in the last equation use has been made of the continuity equation $\nabla\cdot j(x) = -i[H,\rho(x)]$, and of the fact that the initial and final states are eigenstates of the Hamiltonian. In particular, for elastic scattering ($J_f{=}J_i$) the reduced matrix elements of $T^{\rm Coul}_{JM}(q)$ and $T^{\rm Mag}_{JM}(q)$ are proportional to the ground-state charge and magnetic moments, defined as

$$Q_J \equiv \langle J_i, M_i{=}J_i|Q_{J0}|J_i, M_i{=}J_i\rangle \ , \tag{105}$$

$$\mu_J \equiv 2\,m\,\langle J_i, M_i{=}J_i|\mu_{J0}|J_i, M_i{=}J_i\rangle \ , \tag{106}$$

where the magnetic moments μ_J are in terms of nuclear magnetons μ_N. It is then easily found that:

$$\langle J_i||T^{\rm Coul}_J||J_i\rangle \simeq \sqrt{\frac{2J+1}{4\pi}}\frac{\sqrt{2J_i+1}}{\langle J_iJ_i, J0|J_iJ_i\rangle}\frac{q^J}{(2J+1)!!}Q_J \ , \tag{107}$$

$$\langle J_i||T^{\rm Mag}_J||J_i\rangle \simeq -\frac{1}{i}\sqrt{\frac{2J+1}{4\pi}}\sqrt{\frac{J+1}{J}}\frac{\sqrt{2J_i+1}}{\langle J_iJ_i, J0|J_iJ_i\rangle}\frac{q^J}{(2J+1)!!}\frac{\mu_J}{2m} \ , \tag{108}$$

where J satisfies the condition $0 \le J \le 2\,J_i$, and is even in Eq. (107), while it is odd in Eq. (108). In particular, it is found that

$$\langle J_i||T^{\rm Coul}_{J=0}(q)||J_i\rangle \simeq \sqrt{\frac{2J_i+1}{4\pi}}Z \ , \tag{109}$$

and for $J_i \ge 1$

$$\langle J_i||T^{\rm Coul}_{J=2}(q)||J_i\rangle \simeq \frac{1}{6\sqrt{5\pi}}\sqrt{\frac{(J_i+1)(2J_i+1)(2J_i+3)}{J_i(2J_i-1)}}q^2Q_{J=2} \ , \tag{110}$$

where $2\,Q_{J=2}$ is the usual ground-state electric quadrupole moment, while for $J_i \ge 1/2$

$$\langle J_i||T^{\rm Mag}_{J=1}(q)||J_i\rangle \simeq -\frac{1}{i}\frac{1}{\sqrt{6\pi}}\sqrt{\frac{(J_i+1)(2J_i+1)}{J_i}}\frac{q}{2m}\mu_{J=1} \ , \tag{111}$$

where $\mu_{J=1}$ is the usual ground-state magnetic dipole moment.

5.2 The A=3 and 4 systems

Because of a destructive interference in the matrix elements for the magnetic dipole transition between the S- and D-state components of the wave functions, the impulse approximation (IA) predictions for the ^{3}H and ^{3}He magnetic form factors (MFF) have distinct minima at around 3.5 fm^{-1} and 2.5 fm^{-1}, respectively, in disagreement with the experimental data [100–109]. The situation is closely related to that of the backward cross section for electro-disintegration of the deuteron, which is in fact dominated by two-body current contributions for values of momentum transfer above 2.5 fm^{-1}.

The calculated MFF [88] of ^{3}H and ^{3}He are compared with the experimental data in Fig. 10. The ground-state wave functions have been calculated either with the correlated hyperspherical harmonics (CHH) method using the AV18/IX model and including one and two Δ-isobar admixtures with the transition-correlation-operator technique [110]. The AV18/IX ^{3}H and ^{3}He wave functions give binding energies and charge radii, which reproduce the experimental values [94].

While the measured ^{3}H MFF is in excellent agreement with theory over a wide range of momentum transfers, there is a significant discrepancy between the measured and calculated values of the ^{3}He MFF in the region of the diffraction minimum. This discrepancy persists even when different parametrizations of the nucleon electromagnetic form factors are used for the single nucleon current and the model-independent two-body currents.

In Figs. 11–12 the calculated ^{3}H, ^{3}He and ^{4}He charge form factors (CFF) [88,111] are compared with the experimental data [100–109,112]. Note that the four-nucleon wave function is that obtained in a VMC calculation corresponding to the older AV14/VIII model, which underestimates the ^{4}He binding energy by 3 % [53].

The calculated CFF for both A=3 and 4 nuclei are found to be in excellent agreement with the experimental data: the important role of the two-body charge operator contributions above $\simeq$ 3 fm^{-1} is evident, consistently with what was found in earlier studies.

5.3 The A=6 systems

In this section we discuss the ^{6}Li ground-state longitudinal and transverse form factors as well as transition form factors to the excited states with spin, parity and isospin assignments (J^π;T) given by (3^+;0) and (0^+;1). The calculations are based on VMC wave functions obtained from the AV18/IX Hamiltonian model [5,47]. The calculated binding energies for the ground-state, and (3^+;0) and (0^+;1) low-lying excited states are given in Fig. 6. The ground-state is underbound by nearly 4 MeV compared to experiment, and is only 0.4 MeV more bound than the corresponding ^{4}He calculation (27.8 MeV). This is above the threshold for breakup of ^{6}Li into a α-particle and deuteron. In principle, it should be possible to lower the variational energy at least to that threshold, but the wave function would be too spread out. In the variational calculations reported by Wiringa and Schiavilla [113] the parameter search was constrained to keep the rms radius close to the experimental value of 2.43 fm^{-1}. The (exact) GFMC results for this Hamiltonian, also given in Fig. 6, indicate the ground-state binding energy and radius are in agreement with the experimental value, while the (3^+;0) and (0^+;1) experimental binding energies are underestimated by about 3%.

It should be emphasized that previous calculations of the elastic and inelastic six-body form factors have relied on relatively simple shell-model [114–116] or α-d [117] cluster wave functions. These calculations have typically failed to provide a satisfactory, quantitative description of all measured form factors. More phenomenologically successful models have been based on αNN [118–121] clusterization, or on extensions of the basic α-d model with spherical clusters, in which the deuteron is allowed to deform, or stretch, along a line connecting the clusters' centers of mass [122]. However, while these models do provide useful insights into the structure of the A=6 nuclei, their connection with the underlying two- (and three-) nucleon dynamics is rather tenuous.

The calculated elastic form factors $F_L(Q)$ and $F_T(Q)$ [113] are compared

with the experimental values [122–124] in Figs. 13 and 14. Since the ^{6}Li ground-state is (1^+;0), both J=0 and J=2 Coulomb multipoles contribute to F_L, while only the J=1 magnetic multipole operator contributes to F_T. In these figures the results obtained in both IA (empty squares) and with inclusion of two-body corrections in the charge and current operators (filled squares) are displayed, along with the statistical errors associated with the Monte Carlo integrations. The F_L form factor is in excellent agreement with experiment. In particular, the two-body contributions (predominantly due to the π-like charge operator) shift the minimum to lower values of momentum transfer Q, consistently with what has been found for the charge form factors of the hydrogen and helium isotopes. The $T_2^{\rm Coul}$ multipole contribution is much smaller than the $T_0^{\rm Coul}$ one, and at low Q is proportional to the ground-state quadrupole moment. The theoretical prediction for the latter is significantly larger (though with a 50% statistical error) in absolute value than the measured value, but it does have the correct (negative) sign. It is interesting to point out that cluster models of the ^{6}Li ground-state give large, positive values for the quadrupole moment, presumably due to the lack of D-waves in the α-particle, and the consequent absence of destructive interference between these and the D-wave in the α-d relative motion.

The experimental transverse form factor is not well reproduced by theory for Q-values larger than 1 fm^{-1}. Since the ^{6}Li ground-state has T=0, only isoscalar two-body currents contribute to $F_T(Q)$. The associated contributions are small at low Q, but increase with Q, becoming significant for $Q > 3$ fm^{-1}. However, the data cover the Q-range 0–2.8 fm^{-1}. The observed discrepancy between theory and experiment might be due to deficiencies in the VMC wave function. Indeed, it will be interesting to see whether this discrepancy is resolved by using the more accurate GFMC wave functions. We also note that the calculated magnetic moment is about 4 % larger than the experimental value, which is close to that of a free deuteron.

The measured longitudinal inelastic form factor to the (3^+;0) state [125–127] is found to be in excellent agreement with the VMC predictions [113], as can be seen in Fig. 15 . We note that this transition is induced by J=2 and J=4 Coulomb multipole operators, and thus the associated form factor $F_L^2(Q)$ behaves as Q^4 at low Q. Also good agreement between the experimental [127,128] and VMC calculated [113] values is found for the transverse inelastic form factor to the state (0^+;1), Fig. 16 . The latter is an isovector magnetic dipole transition and, as expected, is significantly influenced, even at low values of Q, by two-body contributions, predominantly by those due to the π-like current operator.

5.4 Some concluding remarks

In this section the electromagnetic structure of the A=3–6 nuclei has been discussed within a realistic approach to nuclear dynamics, based on nucleons interacting via two- and three-body potentials and consistent two-body currents. The only phenomenological input, beyond that provided by the underlying interactions, consists of the electromagnetic form factors of the nucleon, which are taken from experiment. Within this framework, a variety of electronuclear observables, including ground-state moments (see Ref. [1]) as well as elastic and inelastic form factors, are reasonably well described by theory at a quantitative level. The only remaining discrepancy is that between the experimental and calculated positions of the first zero in the ^{3}He magnetic form factor and the experimental and calculated transverse form factor of ^{6}Li for Q-values larger than 1 fm^{-1}.

The special role played by the two-body charge and current operators associated with π-exchange should be emphasized. Their contributions dominate both isoscalar and isovector charge form factors of the A=2–4 nuclei, as well as their isovector magnetic structure at intermediate values of momentum transfers $Q \simeq$3.5–4.5 fm^{-1}. In fact, a description in which the degrees of freedom associated with virtual pion production were to be ignored, would dramatically fail to reproduce the experimental data. That only the π-exchange currents required by gauge invariance (and chiral symmetry) should have (so far) clear experimental evidence is perhaps not surprising. This fact has been referred to in the past as the "chiral filter" paradigm [129].

Finally, the remarkable success of the present picture based on (essentially) non-relativistic dynamics, even at large values of momentum transfer, should be stressed. It suggests, in particular, that the present model for the two-body charge operators is better than one *a priori* should expect. These operators, such as the π-exchange charge operator, fall into the class of relativistic corrections. Thus evaluating their matrix elements with the usual non-relativistic wave functions represents only the first approximation to a systematic reduction. A consistent treatment of these relativistic effects would require, for example, inclusion of the boost corrections on the nuclear wave functions [97]. Yet, the excellent agreement between the calculated and measured charge form factors of the A=3–6 nuclei suggests that these corrections may be negligible in the Q-range explored so far.

Acknowledgments

We like to thank our collaborators J. Carlson, J.L. Forest, A. Kievsky, V.R. Pandharipande, D.O. Riska, S. Rosati, M. Viviani, and R.B. Wiringa for their many contributions to the subject of these lectures. The support of the U.S. Department of Energy is gratefully acknowledged. L.E.M. also thanks Jefferson Lab for support via a graduate research assistantship. Many of the calculations reported here were made possible by grants of computer time from the National Energy Research Supercomputer Center.

Tables

Table 1: Experimental deuteron properties compared to recent NN interaction models; meson exchange effects in μ_d and Q_d are not included.

	Experiment	Argonne v_{18}	Nijm-II	Reid93	CD-Bonn	Units
A_S	0.8846(8) [130]	0.8850	0.8845	0.8853	0.8845	fm$^{1/2}$
η	0.0256(4) [131]	0.0250	0.0252	0.0251	0.0255	
r_d	1.971(5) [132]	1.967	1.9675	1.9686	1.966	fm
μ_d	0.857406(1) [133]	0.847				μ_0
Q_d	0.2859(3) [134]	0.270	0.271	0.270	0.270	fm^2
P_d		5.76	5.64	5.70	4.83	

Figures

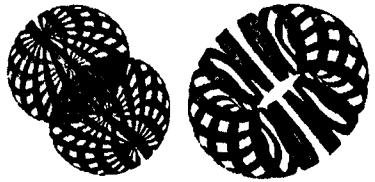

Figure 1: Nucleon densities of the S=1 deuteron in its two spin projections, S_z=±1 and S_z=0, respectively.

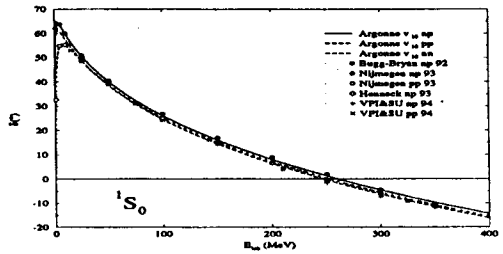

Figure 2: $^1S_0$ phases of the Argonne v_{18} interaction compared to various np and pp phase shift analyses.

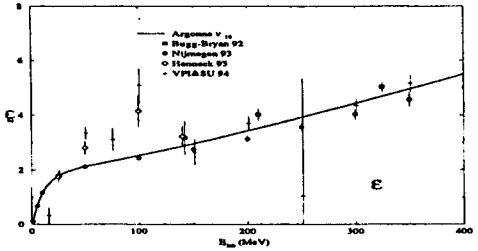

Figure 3: $^3S_1$-$^3D_1$ mixing parameter ϵ_1 from the Argonne v_{18} interaction and various phase shift analyses.

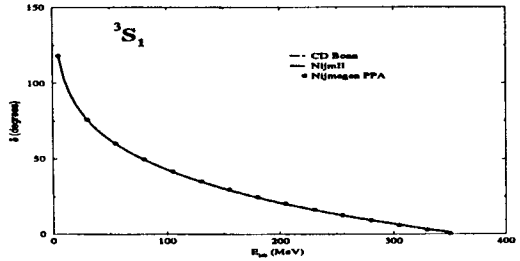

Figure 4: $^3S_1$ phases from different modern NN interaction models.

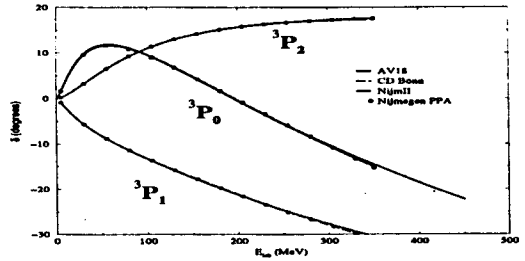

Figure 5: ^3P_J phases from different modern NN interaction models.

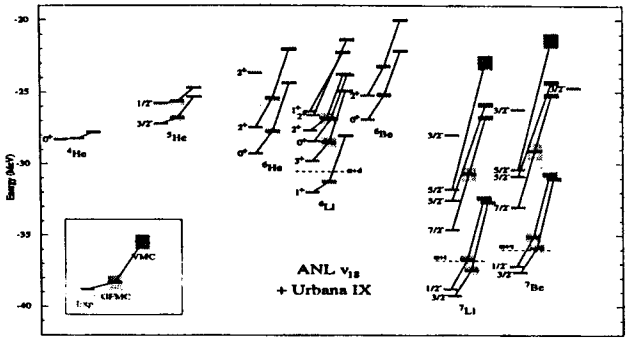

Figure 6: Energy spectra of A=4–7 nuclei, obtained in VMC and GFMC calculations with the Argonne v_{18} two-nucleon and Urbana IX three-nucleon interactions. Both the central value and the one-standard deviation error estimate are shown. GFMC results are a variational bound obtained by averaging from τ=0.04–0.06 MeV^{-1}.

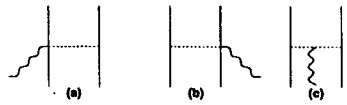

Figure 7: Feynman diagram representation of the isovector two-body currents associated with pion exchange. Solid, dashed, and wavy lines denote nucleons, pions, and photons, respectively.

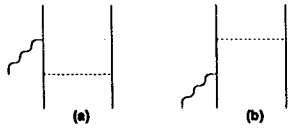

Figure 8: Feynman diagram representation of the Born amplitudes for photoproduction of virtual mesons. Solid, dashed and wavy lines denote nucleons, mesons, and photons, respectively.

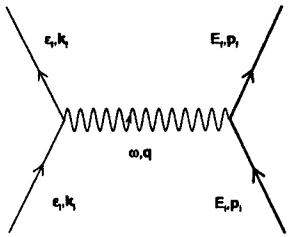

Figure 9: Electron scattering in the one-photon-exchange approximation. Solid, thick-solid and wavy lines denote electrons, hadrons, and photons, respectively.

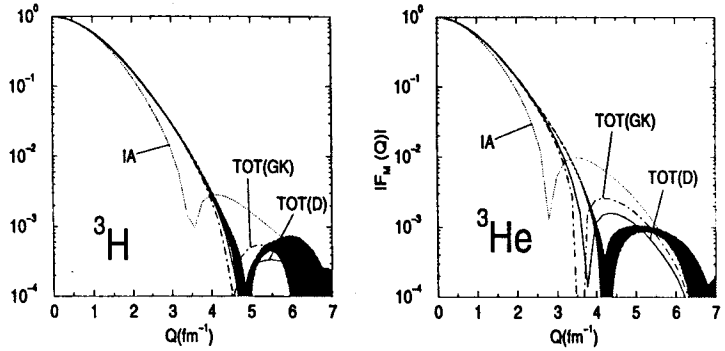

Figure 10: The magnetic form factors of ^{3}H and ^{3}He obtained in impulse approximation (IA), and with inclusion of two-body [TOT(D)] current contributions, are compared with data (shaded area) from Amroun *et al.*[109]. Theoretical results correspond to the AV18/UIX CHH wave functions, and employ the dipole parametrization for the nucleon electromagnetic form factors. Note that the Sachs form factor $G_E^V(q_\mu^2)$ is used in the model-independent isovector two-body currents obtained from the charge-independent part of the AV18 interaction. Also shown are the total results corresponding to the Gari-Krümpelmann parametrization [79] of the nucleon electromagnetic form factor [TOT(GK)].

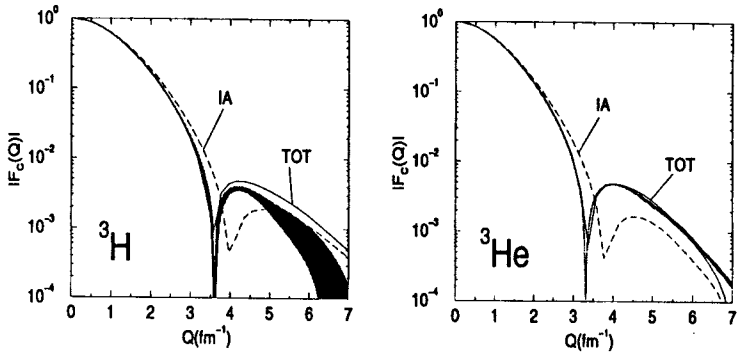

Figure 11: The charge form factors of ^{3}H and ^{3}He, obtained in impulse approximation (IA) and with inclusion of two-body charge operator contributions (TOT), are compared with data (shaded area) from Amroun *et al.*[109]. Note that the IA results also include the Darwin-Foldy and spin-orbit corrections. Theoretical results correspond to the AV18/UIX CHH wave functions, and employ the dipole parametrization of the nucleon electromagnetic form factors.

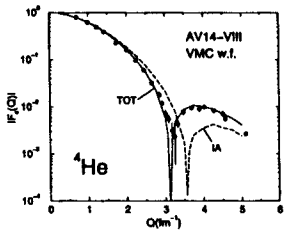

Figure 12: The charge form factors of ^{4}He, obtained in impulse approximation (IA) and with inclusion of two-body charge contributions and relativistic corrections (TOT), are compared with data from Refs.[102,112]. Theoretical results correspond to the Argonne v_{14} two-nucleon and Urbana VIII three-nucleon interactions, use a VMC ^{4}He wave function, and employ the dipole parametrization for the nucleon electromagnetic form factors[111].

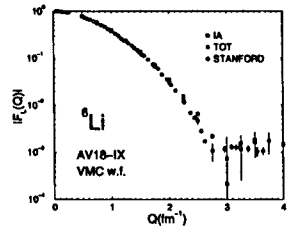

Figure 13: The longitudinal form factors of ^{6}Li, obtained in impulse approximation (IA) and with inclusion of two-body charge operator contributions and relativistic corrections (TOT), are compared with data from Ref.[123]. The theoretical results correspond to the Argonne v_{18} and Urbana IX three-nucleon interactions, use a VMC ^{6}Li wave function, and employ the dipole parametrization of the nucleon electromagnetic form factors[113].

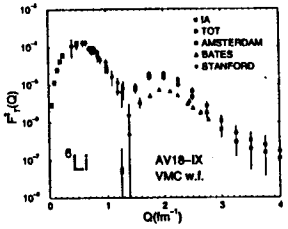

Figure 14: The transverse form factors of ^{6}Li, obtained in impulse approximation (IA) and with inclusion of two-body current contributions (TOT), are compared with data from Refs.[122,124,135]. The theoretical results correspond to the Argonne v_{18} and Urbana IX three-nucleon interactions, use a VMC ^{6}Li wave function, and employ the dipole parametrization of the nucleon electromagnetic form factors[113].

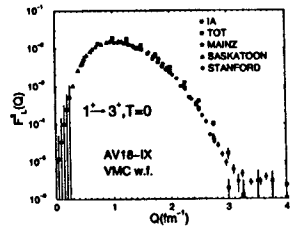

Figure 15: The longitudinal form factors for the transition from the 1^+,T=0 to the 3^+,T=0 (2.18 MeV) levels of ^{6}Li, obtained in impulse approximation (IA) and with inclusion of two-body charge operator contributions and relativistic corrections (TOT), are compared with data from[117]. The theoretical results correspond to the Argonne v_{18} and Urbana IX three-nucleon interactions, use VMC 1^+,T=0 and 3^+,T=0 ^{6}Li wave functions, and employ the dipole parametrization of the nucleon electromagnetic form factors[113].

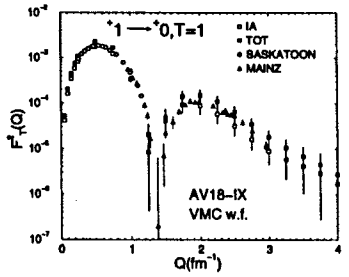

Figure 16: The transverse form factors for the transition from the 1^+,T=0 to the 0^+,T=1 (3.56 MeV) levels of ^{6}Li, obtained in impulse approximation (IA) and with inclusion of two-body current contributions (TOT), are compared with data from [127]. The theoretical results correspond to the Argonne v_{18} and Urbana IX three-nucleon interactions, use VMC 1^+,T=0 and 0^+,T=1 ^{6}Li wave functions, and employ the dipole parametrization of the nucleon electromagnetic form factors [118].

References

1. J. Carlson, and R. Schiavilla, preprint JLAB-THY-97-20, Rev. Mod. Phys. in press (1998).
2. S. Weinberg, Nucl. Phys. B **363**, 3 (1991).
3. R. Machleidt, Adv. Nucl. Phys. **19**, 189 (1989).
4. J. L. Forest, *et al.*, Phys. Rev. C **54**, 646 (1996).
5. R. B. Wiringa, G. J. Stoks, and R. Schiavilla, Phys. Rev. C **51**, 38 (1995).
6. W. N. Cottingham, *et al.*, Phys. Rev. D **8**, 800 (1973).
7. R. Machleidt, K. Holinde, and Ch. Elster, Phys. Rep. **149**, 1 (1987).
8. M. M. Nagels, T. A. Rijken, and J. J. de Swart, Phys. Rev. D **17**, 768 (1978).
9. R. B. Wiringa, R. A. Smith, and T. L. Ainsworth, Phys. Rev. C **29**, 1207 (1984).
10. R. A. Arndt, L. D. Roper, R. L. Workman, and M. W. McNaughton, Phys. Rev. D **45**, 3995 (1992).
11. V. G. J. Stoks, R. A. M. Klomp, C. P. F. Terheggen, and J. J. de Swart, Phys. Rev. C **48**, 2950 (1993).

12. V. G. J. Stoks, R. Timmermans, and J. J. de Swart, Phys. Rev. C **47**, 512 (1993).
13. R. A. Arndt, R. L. Workman, and M. M. Pavan, Phys. Rev. C **49**, 2729 (1994).
14. T. E. O. Ericson, *et al.*, Phys. Rev. Lett. **75**, 1046 (1995).
15. R. A. Arndt, I. I. Strakovsky, and R. L. Workman, Phys. Rev. C **52**, 2246 (1995).
16. D. V. Bugg, and R. Machleidt, Phys. Rev. C **52**, 1203 (1995).
17. V. G. J. Stoks, R. A. M. Klomp, C. P. F. Terheggen, and J. J. de Swart, Phys. Rev. C **49**, 2950 (1994).
18. R. Machleidt, F. Sammarruca, and Y. Song, Phys. Rev. C **53**, R1483 (1996).
19. V. G. J. Stoks, and J. J. de Swart, Phys. Rev. C **41**, 1235 (1990).
20. C. van der Leun, and C. Alderliesten, Nucl. Phys. A **380**, 261 (1982).
21. D. V. Bugg, and R. A. Bryan, Nucl. Phys. A **540**, 449 (1992).
22. R. Henneck, Phys. Rev. C **47**, 1859 (1993).
23. J. Fujita, and H. Miyazawa, Progr. Theor. Phys. **17**, 360 (1957).
24. G. Rupp, and J. A. Tjon, Phys. Rev. C **45**, 2133 (1992).
25. F. Gross, J. W. Van Orden, and K. Holinde, Phys. Rev. C **45**, 2094 (1992).
26. A. Stadler, and F. Gross, Phys. Rev. Lett. **78**, 26 (1997).
27. S. A. Coon, and J. L. Friar, Phys. Rev. C **34**, 1060 (1986).
28. J. L. Friar, and S. A. Coon, Phys. Rev. C **49**, 1272 (1994).
29. W. N. Polyzou, and W. Glöckle, Few-Body Syst. **9**, 97 (1990).
30. B. D. Keister, and W. N. Polyzou, Adv. Nucl. Phys. **20**, 225 (1991).
31. W. Glöckle, T.-S. H. Lee, and F. Coester, Phys. Rev. C **33**, 709 (1986).
32. L. L. Foldy, Phys. Rev. **122**, 275 (1961).
33. R. A. Krajcik, and L. L. Foldy, Phys. Rev. D **10**, 1777 (1974).
34. J. L. Friar, Phys. Rev. C **12**, 695 (1975).
35. J. Carlson, V. R. Pandharipande, and R. Schiavilla, Phys. Rev. C **47**, 484 (1993).
36. P. U. Sauer, Nucl. Phys. A **543**, 291c (1992).
37. A. Picklesimer, R. A. Rice, and R. Brandenburg, Phys. Rev. Lett. **68**, 1484 (1992).
38. A. Picklesimer, R. A. Rice and R. Brandenburg, Few-Body Syst. **19**, 47 (1995).
39. S. A. Coon, M. D. Scadron, P. C. McNamee, B. R. Barrett, D. W. E. Blatt, and B. H. J. McKellar, Nucl. Phys. A **317**, 242 (1979).
40. S. A. Coon, and M. T. Peña, Phys. Rev. C **48**, 2559 (1993).

41. A. Stadler, J. Adam, H. Henning, and P. U. Sauer, Phys. Rev. C **51**, 2896 (1995).
42. M. R. Robilotta, and M. P. Isidro Filho, Nucl. Phys. A **414**, 394 (1984).
43. M. R. Robilotta, M. P. Isidro Filho, H. T. Coelho, and T. K. Das, Phys. Rev. C **31**, 646 (1985).
44. M. R. Robilotta, and M. P. Isidro Filho, Nucl. Phys. A **451**, 581 (1986).
45. M. R. Robilotta, Few-Body Syst. Suppl. **2**, 35 (1987).
46. J. Carlson, V. R. Pandharipande, and R. B. Wiringa, Nucl. Phys. A **401**, 59 (1983).
47. B. S. Pudliner, V. R. Pandharipande, J. Carlson, and R. B. Wiringa, Phys. Rev. Lett. **74**, 4396 (1995).
48. R. A. Malfliet, and J. A. Tjon, Nucl. Phys. A **127**, 161 (1969).
49. R. A. Malfliet, and J. A. Tjon, Phys. Lett. B **29**, 391 (1969).
50. N. Metropolis, A. W. Rosenbluth, M. N. Rosenbluth, A. H. Teller, and E. Teller, J. Chem. Phys. **21**, 1087 (1953).
51. R. B. Wiringa, V. Fiks, and A. Fabrocini, Phys. Rev. C **38**, 1010 (1988).
52. A. Arriaga, V. R. Pandharipande, and R. B. Wiringa, Phys. Rev. C **52**, 2362 (1995).
53. R. B. Wiringa, Phys. Rev. C **43**, 1585 (1991).
54. M. H. Kalos, Phys. Rev. **128**, 1791 (1962).
55. J. Carlson, Phys. Rev. C **36**, 2026 (1987).
56. J. Carlson, Phys. Rev. C **38**, 1879 (1988).
57. J. Carlson, Nucl. Phys. A **522**, 185c (1991).
58. B. S. Pudliner, V. R. Pandhariande, J. Carlson, S. C. Pieper, and R. B. Wiringa, Phys. Rev. C **56**, 1720 (1997).
59. J. B. Anderson, J. Chem. Phys. **63**, 1499 (1975).
60. D. M. Ceperley, and B. J. Alder, Phys. Rev. Lett. **45**, 566 (1980).
61. S. Zhang, J. Carlson, and J. E. Gubernatis, Phys. Rev. Lett. **74**, 3652 (1995).
62. D. O. Riska, Prog. Part. Nucl. Phys. **11**, 199 (1984).
63. M. Chemtob, and M. Rho, Nucl. Phys. A **163**, 1; **212**, 628(E) (1971).
64. D. O. Riska, Phys. Scr. **31**, 107 (1985).
65. D. O. Riska, Phys. Scr. **31**, 471 (1985).
66. D. O. Riska, and M. Poppius, Phys. Scr. **32**, 581 (1985).
67. P. G. Blunden, and D. O. Riska, Nucl. Phys. A **536**, 697 (1992).
68. K. Tsushima, D. O. Riska, and P. G. Blunden, Nucl. Phys. A **559**, 543 (1993).
69. A. Buchmann, W. Leidemann, and H. Arenhövel, Nucl. Phys. A **443**, 726 (1985).
70. K. Ohta, Nucl. Phys. A **495**, 564 (1989).

71. K. Ohta, Phys. Rev. C **39**, 2302 (1989).
72. J. D. Bjorken, and S. D. Drell, *Relativistic Quantum Mechanics* (McGraw-Hill, New York, NY, 1964).
73. T. deForest, and J. D. Walecka, Adv. Phys. **15**, 1 (1966).
74. J. L. Friar, Ann. Phys. **81**, 332 (1973).
75. R. G. Sachs, Phys. Rev. **126**, 2256 (1962).
76. S. Galster, *et al.*, Nucl. Phys. B **32**, 221 (1971).
77. F. Iachello, A. D. Jackson, and A. Lande, Phys. Lett. B **43**, 191 (1973).
78. G. Höhler, *et. al.*, Nucl. Phys. B **114**, 505 (1976).
79. M. Gari, and W. Krümpelmann, Phys. Lett. B **173**, 10 (1986).
80. P. N. Kirk, Phys. Rev. D **8**, 63 (1973).
81. F. Borkowski, *et al.*, Z. Phys. A **275**, 29; Nucl. Phys. B **93**, 461 (1975).
82. G. Simon, *et al.*, Z. Naturforsch. **35** A, 1 (1980).
83. R. C. Walker, *et al.*, Phys. Lett. B **224**, 353 (1989).
84. W. Albrecht, *et al.*, Phys. Lett. B **26**, 642 (1968).
85. S. Rock, *et al.*, Phys. Rev. Lett. **49**, 1139 (1982).
86. S. Platchkov, *et al.*, Nucl. Phys. A **510**, 740 (1990).
87. M. Gari, and W. Krümpelmann, Phys. Lett. B **274**, 159 (1992).
88. L. E. Marcucci, D. O. Riska, and R. Schiavilla, preprint JLAB-THY-98-21, submitted to Phys. Rev. C (1998).
89. R. G. Sachs, Phys. Rev. **74**, 433; **75**, 1605(E) (1948).
90. E. M. Nyman, Nucl. Phys. B **1**, 535 (1967).
91. F. Gross, and H. Henning, Nucl. Phys. A **537**, 344 (1992).
92. R. Schiavilla, V. R. Pandharipande, and D. O. Riska, Phys. Rev. C **40**, 2294 (1989).
93. R. Schiavilla, and D. O. Riska, Phys. Rev. C **43**, 437 (1991).
94. M. Viviani, R. Schiavilla, and A. Kievsky, Phys. Rev. C **54**, 534 (1996).
95. R. Schiavilla, and M. Viviani, to be published (1996).
96. J. Carlson, D. O. Riska, R. Schiavilla, and R. B. Wiringa, Phys. Rev. C **42**, 830 (1990).
97. J. L. Friar, Ann. Phys. **104**, 380 (1977).
98. R. Schiavilla, *Perspectives in Nuclear Physics at Intermediate Energies*, edited by S. Boffi, C. Ciofi degli Atti, and M. M. Giannini (World Scientific, Singapore, 1996).
99. T. W. Donnelly, and I. Sick, Rev. Mod. Phys. **56**, 461 (1984).
100. H. Collard, *et al.*, Phys. Rev. **138**, 357 (1965).
101. J. S. McCarthy, I. Sick, and R. R. Whitney, Phys. Rev. C **15**, 1396 (1977).
102. R. G. Arnold, *et al.*, Phys. Rev. Lett. **40**, 1429 (1978).
103. Z. M. Szalata, *et al.*, Phys. Rev. C **15**, 1200 (1977).

104. J. M. Cavedon, *et al.*, Phys. Rev. Lett. **49**, 978 (1982).
105. P. C. Dunn, *et al.*, Phys. Rev. C **27**, 71 (1983).
106. C. R. Ottermann, *et al.*, Nucl. Phys. A **435**, 688 (1985).
107. F. P. Juster, *et al.*, Phys. Rev. Lett. **55**, 2261 (1985).
108. D. H. Beck, *et al.*, Phys. Rev. Lett. **59**, 1537 (1987).
109. A. Amroun, *et al.*, Nucl. Phys. A **579**, 596 (1994).
110. R. Schiavilla, R. B. Wiringa, V. R. Pandharipande, and J. Carlson, Phys. Rev. C **45**, 2628 (1992).
111. M. J. Musolf, R. Schiavilla, and T. W. Donnelly, Phys. Rev. C **50**, 2173 (1994).
112. R. F. Frosch, *et al.*, Phys. Rev. **160**, 874 (1968).
113. R. B. Wiringa, and R. Schiavilla, to be published (1996).
114. T. W. Donnelly, and J. D. Walecka, Phys. Lett. B **44**, 330 (1973).
115. J. D. Vergados, Nucl. Phys. A **220**, 259 (1974).
116. J. C. Bergstrom, Phys. Rev. C **11**, 1514 (1975).
117. J. C. Bergstrom, Nucl. Phys. A **327**, 458 (1979).
118. V. I. Kukulin, V. T. Voronchev, T. D. Kaipov, and R. A. Eramzhyan, Nucl. Phys. A **517**, 221 (1990).
119. V. I. Kukulin, V. N. Pomerantsev, Kh. D. Razikov, V. T. Voronchev, and G. G. Ryzhikh, Nucl. Phys. A **586**, 151 (1995).
120. D. R. Lehman, and W. C. Parke, Phys. Rev. Lett. **50**, 98 (1983).
121. D. R. Lehman, and W. C. Parke, Phys. Rev. C **28**, 364 (1983).
122. J. C. Bergstrom, S. B. Kowalski, and R. Neuhausen, Phys. Rev. C **25**, 1156 (1982).
123. G. C. Li, I. Sick, R. R. Whitney, and M. R. Yearian, Nucl. Phys. A **162**, 583 (1971).
124. L. Lapikás, *Proceedings of the Conference on Modern Trends in Elastic Electron Scattering*, edited by C. De Vries (NIKHEF-K, Amsterdam), p. 49 (1978).
125. F. Eigenbrod, Z. Phys. **228**, 337 (1969).
126. J. C. Bergstrom, and E. L. Tomusiak, Nucl. Phys. A **262**, 196 (1976).
127. J. C. Bergstrom, U. Deutschmann, and R. Neuhausen, Nucl. Phys. A **327**, 439 (1979).
128. J. C. Bergstrom, I. P. Auer, and R. S. Hicks, Nucl. Phys. A **251**, 401 (1975).
129. M. Rho, and G. E. Brown, Comments Nucl. Part. Phys. **10**, 201 (1981).
130. T. E. O. Ericson, and M. Rosa-Clot, Nucl. Phys. A **405**, 497 (1983).
131. N. L. Rodning, and L. D. Knutson, Phys. Rev. C **41**, 898 (1990).
132. J. Martorell, D. W. L. Sprung, and D. C. Zheng, Phys. Rev. C **51**, 1127 (1995).

133. I. Lindgren, *Alpha-, Beta-, and Gamma-Ray Spectroscopy*, Vol. 2, edited by K. Siegbahn (Amsterdam), p. 1620 (1965).
134. D. M. Bishop, and L. M. Cheung, Phys. Rev. A **20**, 381 (1979).
135. R. E. Rand, R. F. Frosch, and M. R. Yearian, Phys. Rev. **144**, 859 (1966).